Resonant Tunneling Diode Mixer and Multiplier

by

Wenlei Lian

B.A.Sc., Beijing University of Posts and Telecommunications, China, 1990

THESIS SUBMITTED IN PARTIAL FULFILLMENT OF

THE REQUIREMENT FOR THE DEGREE OF

MASTER OF APPLIED SCIENCE

in the

School of Engineering Science

SIMON FRASER UNIVERSITY

April, 1994

APPROVAL

Name: WenLei Lian

Degree: Master of Applied Science

Title of Thesis: Resonant Tunneling Diode Mixer and Multiplier

Examining Committee:

Chair: John Jones
Graduate Chairman and Associate Professor
School of Engineering Science

Senior Supervisor: _____
Shawn Stapleton, P. Eng.
Associate Professor
School of Engineering Science

Supervisor: _____
Steve Hardy, P. Eng.
Professor
School of Engineering Science

Examiner: _____
M. Parameswaran (Ash)
Assistant Professor
School of Engineering Science

Date Approved: April 12, 1994

PARTIAL COPYRIGHT LICENSE

I hereby grant to Simon Fraser University the right to lend my thesis, project or extended essay (the title of which is shown below) to users of the Simon Fraser University Library, and to make partial or single copies only for such users or in response to a request from the library of any other university, or other educational institution, on its own behalf or for one of its users. I further agree that permission for multiple copying of this work for scholarly purposes may be granted by me or the Dean of Graduate Studies. It is understood that copying or publication of this work for financial gain shall not be allowed without my written permission.

Title of Thesis/Project/Extended Essay

"Resonant Tunneling Diode (RTD) Mixer and Multiplier"

Author:

_____
(signature)

Wenlei Lian
(name)

April 12, 1994
(date)

ABSTRACT

Resonant tunneling diode (RTD) microwave mixer and multiplier circuits were designed, fabricated and tested. Analytical analysis of the performance of the RTD mixer and multiplier circuits were performed based on mathematically modeling the RTD I-V curve. The design of the mixer and multiplier was performed using the simulation package ACADEMY. The RTD mixer and multiplier were designed for an RF output of 14 GHz. Comparisons were made between the analytical, simulated and measured results of the RTD mixer and multiplier circuits.

Three conclusions were drawn from this work: 1) An RTD is useful in microwave mixer and multiplier applications. In comparison to the conventional diodes, an RTD has a stronger non-linearity which allows more efficient harmonic generation with smaller input signal levels. 2) The theoretical analysis provides a quantitative relationship between the output and input parameters, also it is shown that at microwave frequencies, the RTD's parallel capacitor can be neglected compared to its parallel resister. 3) The RTD modeling procedure and the simulation package ACADEMY provided very accurate simulation results.

ACKNOWLEDGEMENTS

I would like to acknowledge my supervisor, Dr. Shawn Stapleton, for directing this work and coming up with many useful suggestions. Mr Sirooj Rambaran who gave me a lot of suggestions on the experiment part. Mr Bill Woods who contributed to all of the cleaning, mounting and wirebonding the RTDs to the mixer and multiplier. Mr. Trent Mckeen's considerate help and his bachelor's thesis have been very important references to the simulation part of this thesis. Also the members of the Microwave/RF group and the Microelectronic device group at SFU whose occasional help was much appreciated.

ABBREVIATIONS

BPF	Band Pass Filter
LPF	Low Pass Filter
NDR	Negative Differential Resistance
RTD	Resonant Tunneling Diode
I-V	Current-voltage
C-V	Capacitance-voltage
LO	Local oscillator
RF	Radio frequency
IF	Intermediate frequency
DC	Direct current
PSD	Power spectrum density

TABLE OF CONTENTS

LIST OF FIGURES

1 INTRODUCTION

1.1 Background of RTD

In the late 1950s, Leo Esaki invented the classic example of a quantum device - tunneling diode. Resonant tunneling diode (RTD) has been the subject of theoretical and experimental studies since 1970 [1]. In 1973 Tsu and Esaki [2] first proposed that a large peak in the tunneling current through the structures should occur when the injected carriers have certain resonant energies. In 1974, RTD was first demonstrated [3] by Esaki, Leroy Chang and Raphael Tsu at IBM, the RTD consists of two potential barriers in series, separated by a potential well. The barriers are thin enough that electrons can tunnel through them into and out of the quantum well. In 1983 Sollner et al. [4] reported the first observations of resonant tunneling at room temperature and of large regions of negative differential resistance at lower temperatures. Since then, RTDs have been widely investigated experimentally because of the presence of sharp negative differential resistance (NDR) in the I-V curve, a lot of research work was done to understand the relationship between the physical structures of RTDs and the unique characteristics of RTD [5-14].

In 1989, an equivalent circuit model [15] which will be shown in section 1.3 was established for an RTD. Due to the fast charge transport [5, 9], and the NDR that exists in its I-V curve, the RTD has shown considerable promise for high-frequency applications. Oscillators using RTDs have been reported by a number of authors [4, 5, 9, 15, 16, 17]. Self-oscillating mixers with conversion gain [18] and frequency multipliers [19] are some applications that have been investigated.

Meanwhile, resonant tunneling devices with multiple negative resistance regions are of considerable interest for a variety of potential applications that could be realized with greatly reduced circuit

complexity [20, 21]. These include ultrahigh-speed analog-to-digital converters, parity-bit generators, and multiple-valued logic [22]. RTDs have attracted considerable attention due to their potential applications in both RF and digital areas.

However, two RTD applications in which little work has been done are in subharmonically pumped (SHP) mixer circuits and multiplier circuits for microwave frequencies. K. Krishnmurthi and D.R. Conn have provided a simple method of estimating the conversion gain of SHP RTD mixers [23], and R.J. Hwu has studied RTD frequency multipliers [24]. R.J. Hwu concluded that: (1) the differential negative resistance allows RTD's efficiencies greater than the limit $1/n^2$ (n is the output harmonic number) for monotonically increasing I-V curves; (2) the Q factor (cutoff frequency f_c / central frequency f_o) is the major parameter on determining the multiplication efficiency of an RTD; (3) the multiplication performance of a negative resistance RTD is determined by the capacitance, series resistance and negative differential resistance at the operating point. Based on the initial work of reference [23, 24], the subject of this thesis will focus on the performance of RTD mixer and multiplier applications for microwave frequencies. The potential performance advantages of RTDs compared to the conventional diodes (Schottky barrier diodes and varactor diodes) in nonlinear microwave applications need to be discussed.

1.2 Schottky Barrier Diode and Varactor Diode

A) Varactor diode

Varactor diode (variable reactance diode) is used as a voltage-variable capacitor, wherein the diode junction capacitance can be changed by varying the reverse bias applied to the diode. A representative circuit of a varactor diode is presented below:

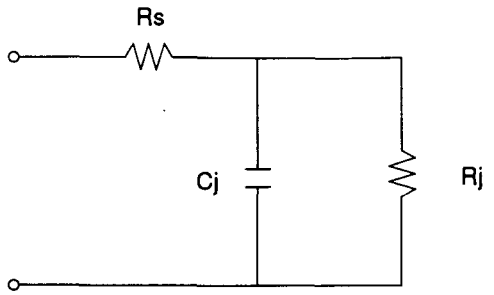

Fig. 1.1 Representative circuit of a varactor diode showing case resistance, junction resistance and junction capacitance

In this equivalent circuit the diode junction consists of junction capacitance C_j and junction resistance R_j. The bulk resistance is shown as R_s. The performance of the diode junction at a particular frequency is determined mainly by C_j and R_s. As the operating frequency is increased, the diode performance degrades, because the transit time established by C_j and R_s. An important characteristic of the varactor diode is the figure of merit Q, which is determined by the ratio of the diode's capacitive reactance X_j and bulk resistance R_s.

Present-day varactor diodes operate into the microwave part of the spectrum. They are quite efficient as frequency multipliers at power levels as great as 25 watts. The efficiency of a correctly designed varactor multiplier exceeds 50% in most instances.

B) Schottky barrier diode

Schottky barrier (silicon hot-carrier) diodes are ideal for VHF and UHF mixer and detector applications. They are readily adaptable to many other fast switching RF and digital applications. They provide stable electrical characteristics by eliminating the point-contact diode presently used in many applications. They have very low capacitance, low noise figure, low series resistance R_s, high forward conductance, high reverse voltage and low reverse leakage. Low barrier Schottky diode is well-suited for applications where -6 dBm to +5 dBm

per diode is available. High barrier Schottky diode is well-suited for mixer applications where +3 dBm to +6 dBm per diode is available, its cutoff frequency is up to 370GHz. The equivalent circuit of Schottky diode is similar to that of the varactor diode.

Daniel et al [25] and Kerr et Al [26] presented analysis for the conversion loss and noise of microwave and millimeter-wave Schottky barrier mixers both in theory and experiment which were in agreement.

C) The comparison of RTD, Schottky barrier diode and varactor diode

By using a device having a symmetric C-V curve or an antisymmetric I-V curve, only odd-harmonics of frequency multiplication with an unbiased RTD are generated due to cancellation of the even harmonics, therefore, there is no need for an idler termination in the case of a frequency tripler (although in this thesis, this advantage hasn't be utilized). Similarly a frequency quintupler requires only one idler termination at the 3rd harmonic for optimum operation, greatly simplifying the circuit design. Schottky barrier and varactor diode having asymmetric curves generally require an idler termination at each intermediate harmonic frequency.

Knowing the potential advantages of an RTD compared to conventional diodes, a more indepth understanding of an RTD is required.

1.3 Physical Structure of RTD

RTD structures consist of two semiconductor barriers 1-5nm thick, embedded in a semiconductor having a smaller band gap energy than that of the barrier material, and separated by 2-6nm. In this way the carriers are confined to the lower band gap material but can readily tunnel through the thin

barriers under an applied bias voltage.

To obtain high quality quantum well structures, a lattice matched heterostructure was employed in our experiment [27]. Shown as Fig. 1.2, being grown on a semi-insulating GaAs substrate, the double barrier quantum well structure consists of two undoped AlGaAs barriers separated by an undoped GaAs quantum well. Next to the two barriers are the undoped GaAs space layers, outside of which are the cathode side and anode side. One the top of the RTD is the ohmic contact and the metallization, at the bottom is the undoped GaAs.

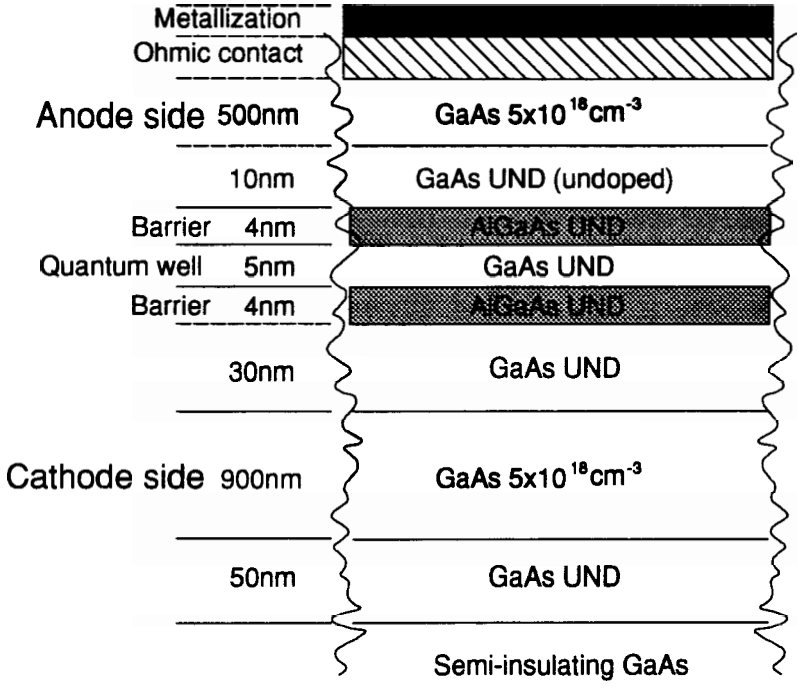

Fig. 1.2 Cross-sectional view of the GaAs/$Al_{0.4}Ga_{0.6}As$ RTD structure

If the total energy and momentum of the electrons in the plane of the heterojunctions in Fig 1.2 are observed, the energy band diagram of the generic double-barrier structure with quasibound-state energy is obtained, shown as below:

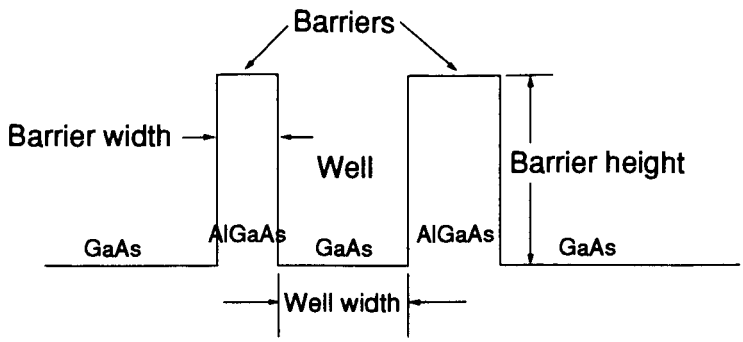

Fig. 1.3 Band diagram of a generic double-barrier structure with quasibound-state energy

There are five physical parameters that can be varied in an RTD: 1) the barrier height, 2) the well depth, 3) the symmetry of the structure, 4) the quantum well width, 5) the barrier width.

1.4 Equivalent Circuit of RTD

The equivalent circuit of the double barrier resonant tunneling diode used for analysis is shown in Figure 1.4 The intrinsic RTD consists of a variable conductance g(v) in parallel with a variable capacitance c(v), followed by a constant series resistor R_S.

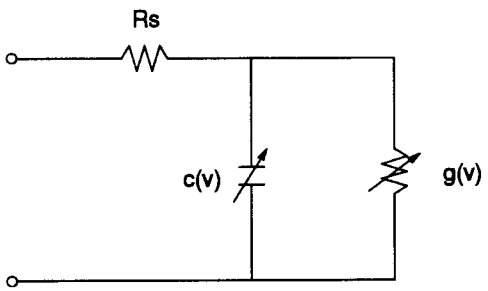

Fig. 1.4 Equivalent circuit of RTD

1.5 Characteristics of RTD

1.5.1 Characteristic I-V Curve of RTD

The typical characteristic DC I-V curve of an RTD is shown in Fig. 1.5. The current initially increases monotonically with the DC bias voltage. The peak current I_P occurs when the energy of most of the incident electrons is in resonance with the energy levels in the well. The current then drops after the resonance is passed till it reaches the valley current I_V. A negative differential resistance (NDR) region is therefore displayed. After the valley point, the current is increasing again. The corresponding voltage of the peak (valley) current of this I-V curve is V_P (V_V). The negative part is almost in odd symmetry with the positive part.

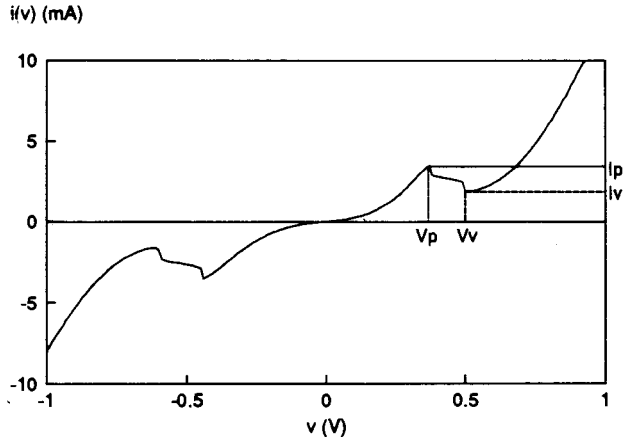

Fig. 1.5 A typical RTD I-V curve

1.5.2 C-V Curve of RTD

The typical C-V curve of the variable capacitance is shown in Fig. 1.6. For the positive part, the capacitance decreases with increased bias at low voltages, followed by a well-defined peak structure and finally declines. The negative part is almost in even symmetry with the positive part.

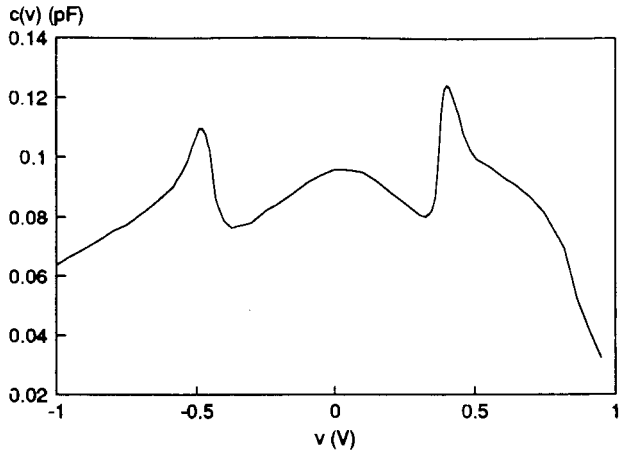

Fig. 1.6 A typical RTD C-V curve

1.5.3 Other Important Characteristic of RTD

An RTD produces a high cutoff frequency due to its low capacitance resulting from the added adjacent region. It has been verified that an RTD can operate very well even at high-frequencies from 30 GHz up to several THz [4].

2 MATHEMATICAL MODEL OF RTD

In order to make it easier to predict the performance of RTD circuits, one need to provide theoretical analysis of the RTD circuits to reveal the relationship between the output results and the input parameters. Among all the parameters that control the performance of the RTD circuits, the RTD I-V and C-V curves play a main role in the analysis, thus mathematical models of RTD I-V and C-V curves need to be developed.

2.1 I-V Curve and Conductance Curve of RTD

To make the theoretical analysis analytically tractable, the I-V curve of an RTD can be mathematically represented as an antisymmetric curve, which consists of two exponential curves and two Gaussian curves:

$$i(v) = k_3 \cdot \left(e^{k_0 \cdot v} - e^{-k_0 \cdot v}\right) + k_1 \cdot \left[e^{-\frac{(v-x_1)^2}{k_2}} - e^{-\frac{(v+x_1)^2}{k_2}}\right] \tag{2-1}$$

where x_1 controls the peak current point (V_P, I_P) position of RTD I-V curve.

k_0 controls the slope of RTD I-V curve.

k_1 controls the peak current value I_P of RTD I-V curve.

k_2 controls the valley current point (V_V, I_V) position of RTD I-V curve.

k_3 is simply a unit transfer constant.

The physical meanings of x_1, k_0, k_1, k_2 and k_3 will be explained more in the next section. The Figure below shows the plot of Eqn. (2-1).

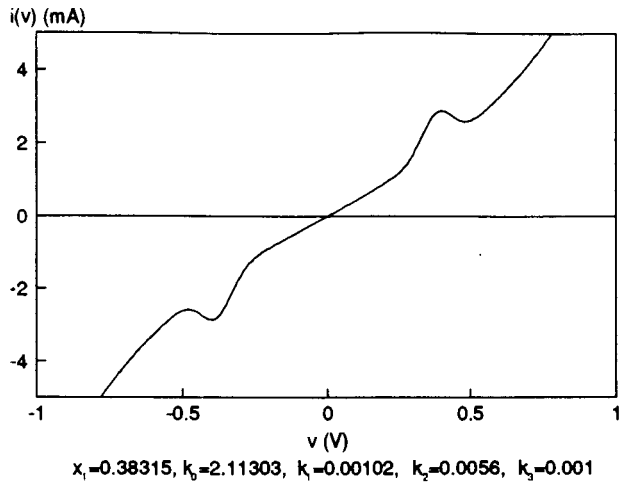

Fig. 2.1 Mathematical model of RTD I-V curve

I_P (I_V) is the peak (valley) current, V_P (V_V) is its corresponding voltage. Some other parameters of RTD I-V curve are: (1) positive region conductance G_P, (2) negative differential region conductance G_D, and (3) peak-to-valley current ratio R_I, which are defined as:

$$G_P = \frac{I_P}{V_P} \tag{2-2}$$

$$G_D = \frac{I_P - I_V}{V_V - V_P} \tag{2-3}$$

$$R_I = \frac{I_P}{I_V} \tag{2-4}$$

Given a peak voltage V_P, with G_P, G_D, and R_I, all the extreme points in an RTD I-V curve are determined.

The conductance of an RTD can be obtained from the derivative of i(v):

$$gg(v) = k_0 \cdot k_3 \cdot \left(e^{k_0 \cdot v} + e^{-k_0 \cdot v}\right) \qquad (2\text{-}5)$$
$$-\frac{2k_1}{k_2} \cdot \left[(v - x_1) \cdot e^{-\frac{(v-x_1)^2}{k_2}} - (v + x_1) \cdot e^{-\frac{(v+x_1)^2}{k_2}}\right]$$

As shown below, the conductance curve of the RTD is even symmetrical.

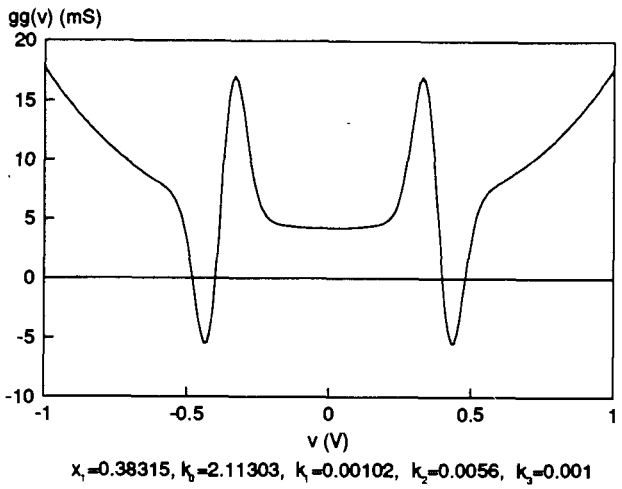

Fig. 2.2 Mathematical conductance curve of RTD

2.2 Physical Meanings of x_1, k_0, k_1, k_2 and k_3

In order to know the physical meanings of x_1, k_0, k_1 and k_2 (or the relationship between the four parameters (k_3=constant) and the other four parameters V_P, G_P, G_D, and R_I), one of the four parameters (x_1, k_0, k_1 and k_2) will be changed, while the other parameters remain at the same values.

1) x_1 parameter

From the I-V curves plotted below, one can tell that x_1 controls the position of the peak current point (V_P, I_P). When x_1 is increased, V_P and I_P are increased and the NDR region is simply shifted, G_P, G_D, and R_I are all decreased.

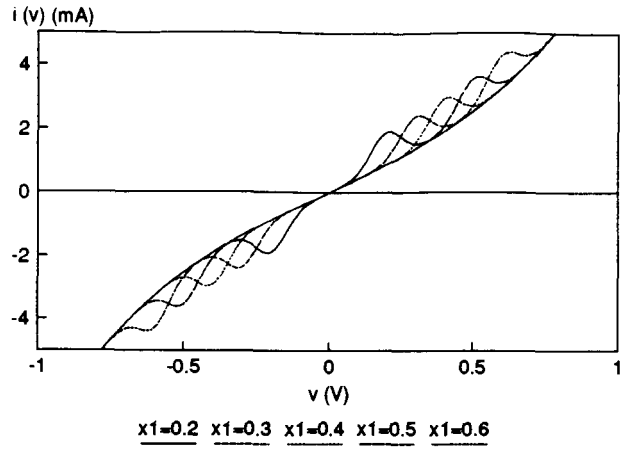

Fig. 2.3 RTD I-V curves with varying x_1 (k_0, k_1 and k_2 remain fixed)

2) k_0 parameter

From the I-V curves plotted below, one can tell that k_0 controls the slope of the RTD I-V curve, when k_0 is increased, G_P increases, but V_P, G_D and R_I all decrease.

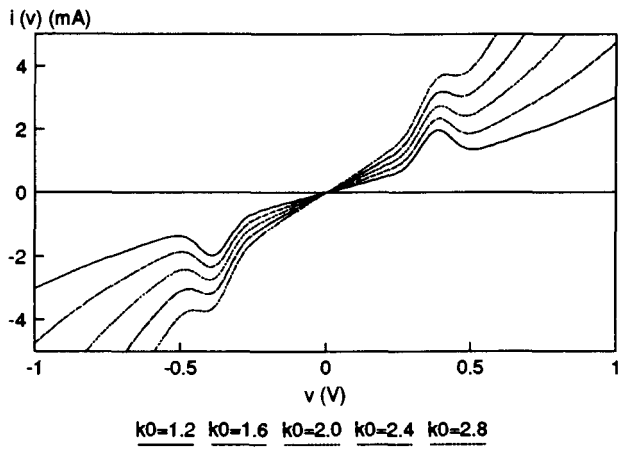

Fig. 2.4 RTD I-V curves with varying k_0 (x_1, k_1 and k_2 remain fixed)

3) k_1 parameter

From the I-V curves plotted below, one can tell that k_1 controls the peak current value I_P. When k_1 is increased, V_P, V_V and I_V remain unchanged, meanwhile G_P, G_D and R_I are all increased.

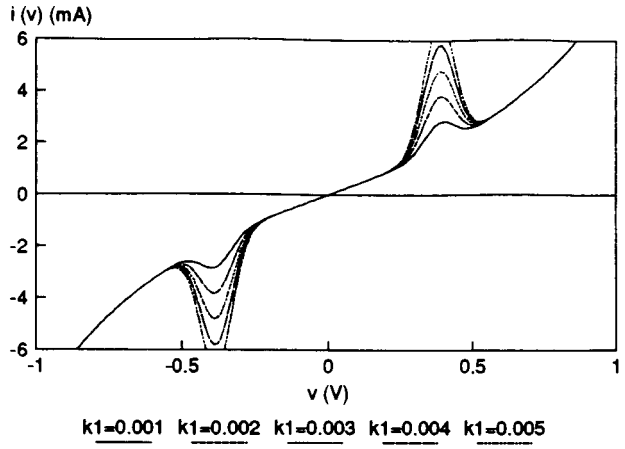

Fig. 2.5 RTD I-V curves with varying k_1 (x_1, k_0 and k_2 remain fixed)

4) k_2 parameter

From the I-V curves plotted below, one can tell that k_2 controls the position of the valley current point (V_V, I_V). When k_2 is increased, the peak current point (V_P, I_P) stays in the same position, while the valley current point shifts along the original I-V curve. G_P will stay the same value, G_D and I_R decrease.

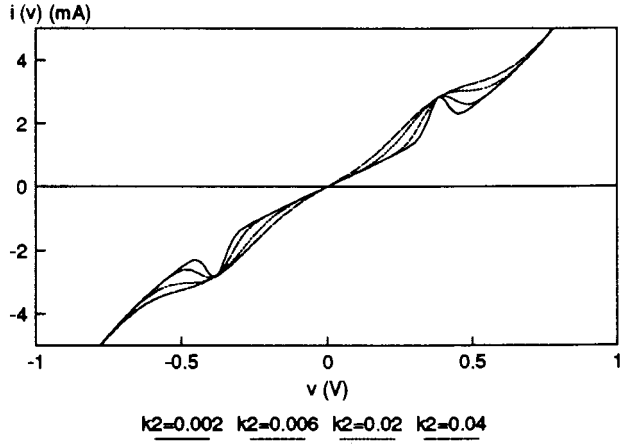

Fig. 2.6 RTD I-V curves with k_2 being changed (x_1, k_0 and k_1 remain fixed)

2.3 C-V Curve of RTD

Again, to simplify the theoretical analysis, the C-V curve of the RTD can be mathematically represented as an even symmetric curve, which is the overlapping of a parabola curve and two Gaussian curves:

$$c(v) = C_0 \cdot (1 - \phi \cdot v^2) + \Delta C \cdot \left[e^{-\frac{(v-V_0)^2}{\Delta V^2} 4\ln(2)} + e^{-\frac{(v+V_0)^2}{\Delta V^2} 4\ln(2)} \right] \tag{2-6}$$

$$\Delta C = C1 - C_0(1 - \phi \cdot V_0^2) \tag{2-7}$$

where C_0 is the capacitance value at zero bias voltage.

C1 is the peak capacitance value.

V_0 is the bias voltage at which the capacitance is C1.

ϕ is the build in voltage potential (≈ 0.7).

ΔV is the voltage difference between the two voltages at which the Gaussian curve and the parabola curve intersect.

The figure below shows the plot of Eqn. (2-6) and (2-7), for a typical RTD.

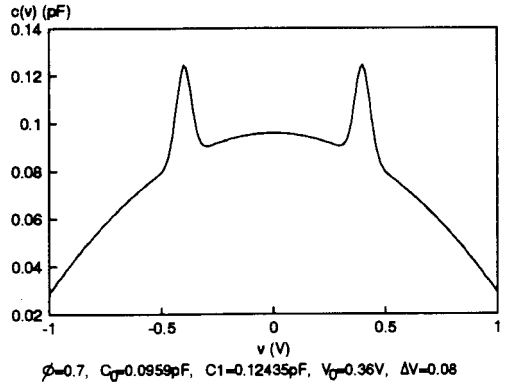

Fig. 2.7 Mathematical model of RTD C-V curve

3 THEORETICAL ANALYSIS OF RTD MIXER AND MULTIPLIER

A mixer is a critical component in modern RF systems. Since it is usually the first or second device from the RF input, the performance of the mixer is crucial to the overall operation of the system. A mixer is a three port device through which a power at one frequency is converted into the power at another frequency. The port through which the input signal enters the mixer is called the input port, the port through which the local oscillator signal enters the mixer is called the LO port, and the port through which all the output products exit the mixer is called the output port. The input and LO signals are mixed by means of nonlinearities and switching to produce a group of signals having frequencies equal to the sums and differences of the harmonics of the input and LO signals, after passing through a filter, the output products are obtained. Also a DC bias is often used for *starved* LO operation. The power efficiency of a mixer is a measure of how efficiently frequency conversion occurs.

A multiplier can be used in many applications, such as phase locked loop, digital circuits, etc. A multiplier is a two port nonlinear harmonic generator, which converts the input signal at certain frequency into its harmonics. The output products at the output port are obtained by passing the input signal through a nonlinear device (diode), and then through a filter. A DC bias is often used for the multiplier to work at a certain point on the I-V curve. The power efficiency of a multiplier is a measure of how efficiently harmonics are generated.

The mathematical models for an RTD (I-V curve, C-V curve) have been obtained in chapter 2, one needs to derive a method to calculate the efficiency of an RTD mixer and multiplier according to the nonlinearity of the RTD. From the conductance-voltage curve (Fig. 2.2) and the C-V curve (Fig. 2.7) model of the RTD, one can compare the admittance of the variable conductance and the variable capacitance at microwave frequency (0.3-30GHz), shown as below:

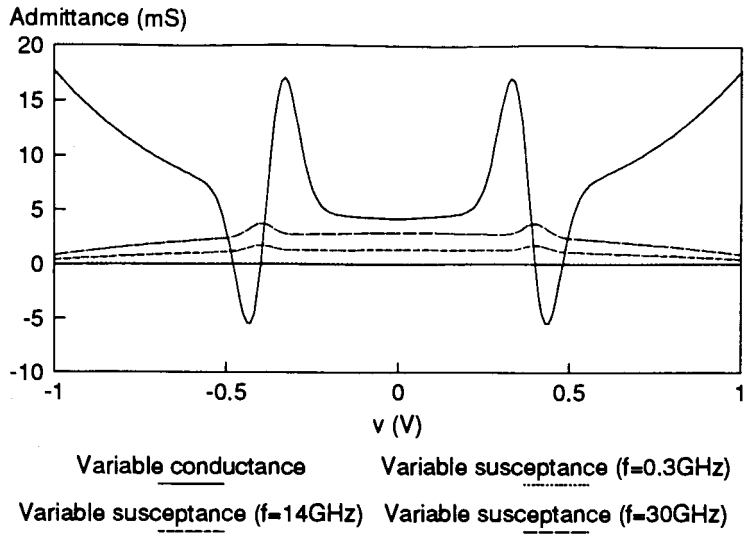

Fig. 3.1 Admittance of the variable conductance and capacitance of the RTD

It is shown that even at the highest microwave frequency (30GHz), the susceptance of the variable capacitance is trivial compared to the conductance of the variable conductance of the RTD. Therefore at microwave frequency, the effect of the variable capacitance inside an RTD can be ignored, and only the characteristic I-V curve of an RTD will be considered in the analysis.

3.1 RTD Mixer

3.1.1 RTD Mixer Configuration

To obtain the efficiency of an RTD mixer, the mixer topology needs to be specified. The RTD mixer configuration most commonly used is the Z mixer, shown as Fig. 3.2. Vb is the DC bias voltage, and R_{IF} and R_{RF} are the source and load impedances, respectively. Vg is the voltage source. The three band pass filters BPF_IF, BPF_RF, BPF_LO are frequency selective networks, whose impedances are zero at f_{IF}, f_{RF}, f_{LO}, respectively, and infinite at all other frequencies. Thus the only voltages which can exist across the diode are the DC bias voltage Vb, V_{LO} at the LO pump frequency f_{LO}, V_{IF} at the IF frequency f_{IF}, and V_{RF} at the RF frequency f_{RF}.

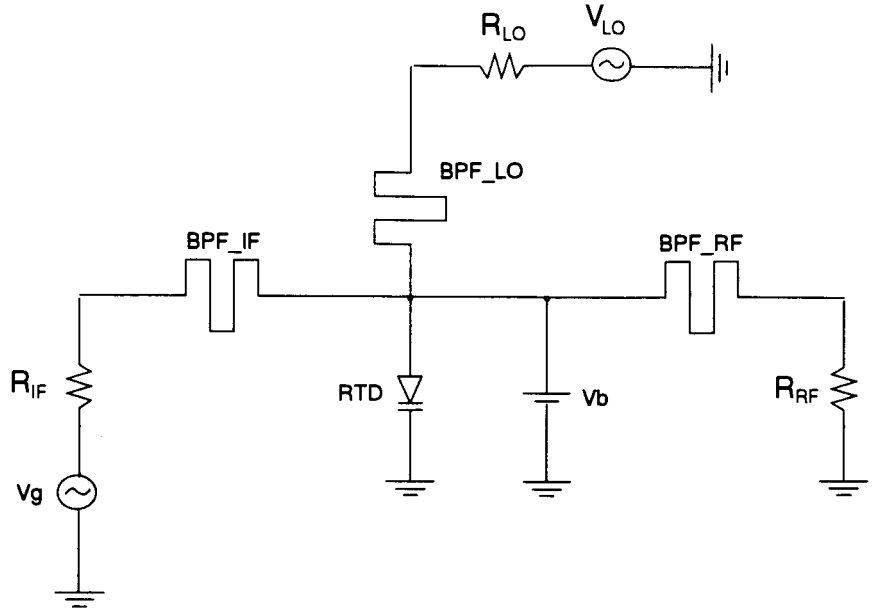

Fig. 3.2 Configuration of the RTD Z mixer showing the IF, RF, and LO ports

Another equivalent mixer configuration is the Y mixer, shown as Fig. 3.3. G_{IF} and G_{RF} are the source and load conductances, respectively, and Ig is the current source. The three stop band filters SBF_IF, SBF_RF, SBF_LO are frequency selective networks, whose admittances are zero at f_{IF}, f_{RF}, f_{LO}, respectively, and infinite at all other frequencies. Thus the only voltages that can exist across the diode are V_{LO} at the pump frequency f_{LO}, V_{IF} at the IF frequency f_{IF}, and V_{RF} at the RF frequency f_{RF}.

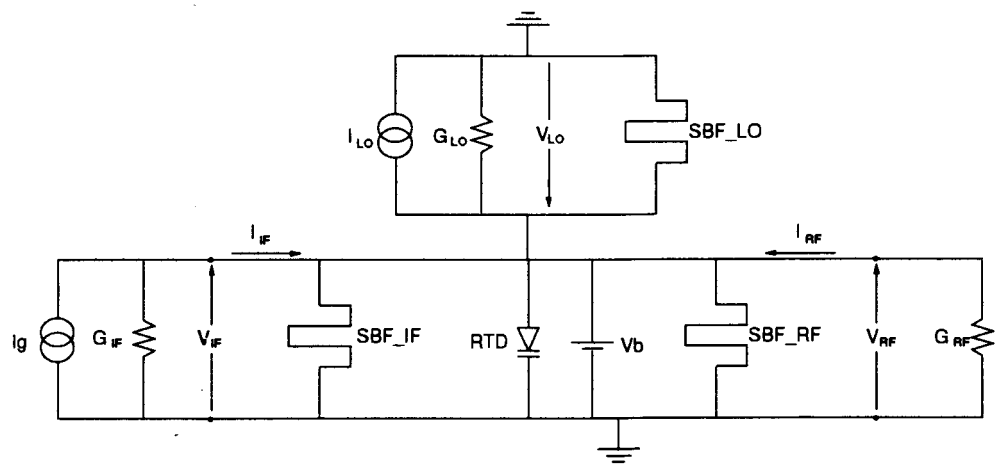

Fig. 3.3 Configuration of the RTD Y mixer showing the RF, IF, and LO ports

3.1.2 RTD Mixer Efficiency

The efficiency of a down-converter mixer is the ratio of the load power at the RF port to the power available from the IF source. From the configuration of the RTD mixer, one should be able to calculate the efficiency of the RTD mixer. The procedure used to obtain an expression for the efficiency of an RTD mixer follows the commonly used method of treating the nonlinear conductance as a DC biased linear time-varying element [29]. Here, the RTD Y mixer configuration is chosen for the analysis. When a local oscillator voltage $v_{LO} = V_{LO}\cos\omega_{LO}t$ and a bias voltage Vb are applied to RTD, the periodically varying device conductance (Eqn. (2-5)) can be expressed as a Fourier series:

$$\begin{aligned} g(\theta) &= gg(Vb + V_{LO}\cdot\cos\theta) \\ &= k_0\cdot k_3\cdot\left[e^{k_0\cdot(Vb+V_{LO}\cdot\cos\theta)} + e^{-k_0\cdot(Vb+V_{LO}\cdot\cos\theta)}\right] \\ &\quad -\frac{2k_1}{k_2}\cdot\left[(Vb+V_{LO}\cdot\cos\theta - x_1)\cdot e^{-\frac{(Vb+V_{LO}\cdot\cos\theta - x_1)^2}{k_2}}\right. \\ &\quad \left. -(Vb+V_{LO}\cdot\cos\theta + x_1)\cdot e^{-\frac{(Vb+V_{LO}\cdot\cos\theta + x_1)^2}{k_2}}\right] \\ &= G_0 + 2G_1\cdot\cos\theta + 2G_2\cdot\cos 2\theta + \cdots \end{aligned} \tag{3-1}$$

Where

$$\theta = \omega_{LO}\cdot t \tag{3-2}$$

$$G_0 = \frac{1}{2\pi}\int_{-\pi}^{\pi} g(\theta)d\theta = \frac{1}{\pi}\int_0^{\pi} g(\theta)d\theta \tag{3-3}$$

$$G_1 = \frac{1}{2\pi}\int_{-\pi}^{\pi} g(\theta)\cdot\cos\theta d\theta = \frac{1}{\pi}\int_{0}^{\pi} g(\theta)\cdot\cos\theta d\theta \tag{3-4}$$

G_2 and higher order terms are neglected, as they produce signals at frequencies other than the frequencies f_{IF} and f_{RF}, and the higher order mixing products are assumed to be short-circuited.

With the conductance coefficients given above, the conversion matrix relating the RF and IF phasor voltages and currents can be formulated.

Let the conductance wave-form be expressed as:

$$g(t) = \sum_{n=-\infty}^{\infty} G_n \cdot e^{j(n\cdot\omega_{LO})\cdot t} \tag{3-5}$$

The voltage across the diode consists of intermodulation products of ω_{IF} and ω_{LO}:

$$v(t) = \sum_{n=-\infty}^{\infty} V_n \cdot e^{j(\omega_{IF}+n\cdot\omega_{LO})\cdot t} \tag{3-6}$$

Similarly the current through the diode can be expressed as:

$$i(t) = \sum_{n=-\infty}^{\infty} I_n \cdot e^{j(\omega_{IF}+n\cdot\omega_{LO})\cdot t} \tag{3-7}$$

The resulting time domain equation is therefore:

$$i(t) = g(t)\cdot v(t) \tag{3-8}$$

We denote the subscript n by the frequency $\omega_n = \omega_{IF} + n\cdot\omega_{LO}$:

:

$n=-1$ --> $\omega_{IF}-\omega_{LO}$: image freq.

$n=0$ --> ω_{IF}: IF freq.

$n=1$ --> $\omega_{IF}+\omega_{LO}:=\omega_{RF}$: RF freq.

$n=2$ --> $\omega_{IF}+2\omega_{LO}$: IF freq.

:

Thus

$$\begin{pmatrix} I_1 \\ I_0 \end{pmatrix} = \begin{pmatrix} I_{RF} \\ I_{IF} \end{pmatrix} \text{ and } \begin{pmatrix} V_1 \\ V_0 \end{pmatrix} = \begin{pmatrix} V_{RF} \\ V_{IF} \end{pmatrix} \tag{3-10}$$

The frequency domain response of Eqn. (3-8) is written:

$$\underline{I} = \underline{G} \cdot \underline{V} \tag{3-11}$$

Where $\underline{I} = \{I_n\}$, $\underline{V} = \{V_n\}$, and $\underline{\mathrm{G}}$ is an $\infty \times \infty$ Hermitan matrix:

$$\begin{matrix} \\ \\ RF \\ IF \\ Image \\ \\ \end{matrix} \begin{bmatrix} \vdots \\ I_{+2} \\ I_{+1} \\ I_0 \\ I_{-1} \\ I_{-2} \\ \vdots \end{bmatrix} = \begin{bmatrix} \vdots & \vdots & \vdots & \vdots & \vdots & \vdots & \vdots \\ \vdots & G_0 & G_1 & G_2 & G_3 & G_4 & \vdots \\ \vdots & G_1^* & G_0 & G_1 & G_2 & G_3 & \vdots \\ \vdots & G_2^* & G_1^* & G_0 & G_1 & G_2 & \vdots \\ \vdots & G_3^* & G_2^* & G_1^* & G_0 & G_1 & \vdots \\ \vdots & G_4^* & G_3^* & G_2^* & G_1^* & G_0 & \vdots \\ \vdots & \vdots & \vdots & \vdots & \vdots & \vdots & \vdots \end{bmatrix} \cdot \begin{bmatrix} \vdots \\ V_{+2} \\ V_{+1} \\ V_0 \\ V_{-1} \\ V_{-2} \\ \vdots \end{bmatrix} \tag{3-12}$$

Because the effect of the capacitance is neglected in this thesis, the conductance is real, and the RF and IF currents can be obtained:

$$\begin{bmatrix} I_{RF} \\ I_{IF} \end{bmatrix} = \begin{bmatrix} G_0 & G_1 \\ G_1 & G_0 \end{bmatrix} \cdot \begin{bmatrix} V_{RF} \\ V_{IF} \end{bmatrix} \tag{3-13}$$

The y parameter matrix can be expressed as a function of the G parameters.

$$\begin{bmatrix} y_{11} & y_{12} \\ y_{21} & y_{22} \end{bmatrix} = \begin{bmatrix} G_0 & G_1 \\ G_1 & G_0 \end{bmatrix} \tag{3-14}$$

The efficiency of an RTD mixer can be calculated from its G parameter matrix, along with the IF and RF load conductances:

$$\eta = \frac{\text{load power at } f_{RF}}{\text{power available from IF source at } f_{IF}} \tag{3-15}$$

$$= \frac{\frac{1}{2} G_{RF} \cdot |V_{RF}|^2}{\left(\frac{1}{2}\frac{I_g}{\sqrt{2}}\right)^2 / G_{IF}} = 4 G_{IF} \cdot G_{RF} \cdot \left| \frac{V_{RF}}{I_g} \right|^2 = 4 G_{IF} \cdot G_{RF} \cdot |Z_{RF,g}|^2$$

Where $Z_{RF,g}$ is the ratio of the RF load voltage to the IF source current, that is, the *transfer impedance* between the input and output ports with the output port open circuited.

From Eqn. (3-14), one can tell that the power efficiency of the RTD mixer is proportional to the square of the source-to-load *transfer impedance* $Z_{RF,g}$. We need to determine an expression for $Z_{RF,g}$ as a function of the known variables (G_0, G_1). From the RTD Y mixer configuration, it's easy to visualize that Fig. 3.3 is actually a two port network consisting of three cascaded two port networks: source two port network EFGH, RTD two port network IJKL and load two port network MNOP. Knowing the source and load conductances (G_{IF}, G_{RF}) and the G parameter matrix of the RTD, the expression for $Z_{RF,g}$ is not difficult to obtain. The RTD Y mixer configuration is redrawn below:

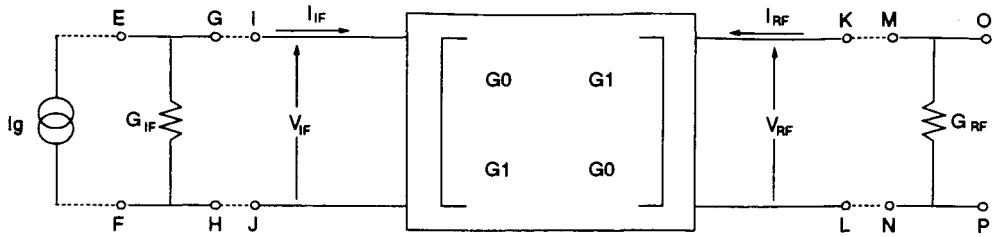

Fig. 3.4 Re-draw of Fig. 3.3 as three cascade two port networks

By incorporating the IF source conductance G_{IF} and the RF load conductance G_{RF} with the RTD two port network, one can evaluate the overall ABCD matrix by multiplying the individual ABCD matrices.

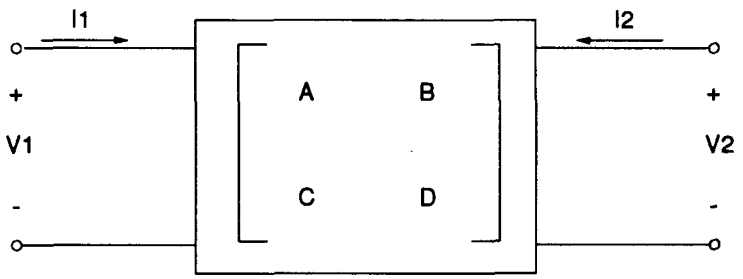

Fig. 3.5 A basic two port network

Shown as Fig. 3.5, from the definition of the ABCD parameters:

$$V_1 = A \cdot V_2 - B \cdot I_2 \tag{3-16}$$

$$I_1 = C \cdot V_2 - D \cdot I_2$$

The two port network ABCD parameters for a shunt conductance G are:

$$\begin{bmatrix} A & B \\ C & D \end{bmatrix} = \begin{bmatrix} 1 & 0 \\ G & 1 \end{bmatrix} \tag{3-17}$$

and the ABCD parameters for the RTD two port network IJKL can be obtained from the transformation of the Y parameters shown in Eqn. (3-14):

$$\begin{pmatrix} A & B \\ C & D \end{pmatrix} = \begin{pmatrix} \frac{-y_{22}}{y_{21}} & \frac{-1}{y_{21}} \\ \frac{-|y|}{y_{21}} & \frac{-y_{11}}{y_{21}} \end{pmatrix} = \begin{pmatrix} \frac{-G_0}{G_1} & \frac{-1}{G_1} \\ \frac{-(G_0^2 - G_1^2)}{G_1} & \frac{-G_0}{G_1} \end{pmatrix} \tag{3-18}$$

Where

$$|y| = y_{11} \cdot y_{22} - y_{12} \cdot y_{21}$$

Thus for the whole cascaded two port network, we can write:

$$\begin{pmatrix} A & B \\ C & D \end{pmatrix} = \begin{pmatrix} 1 & 0 \\ G_{IF} & 1 \end{pmatrix} \cdot \begin{pmatrix} \frac{-G_0}{G_1} & \frac{-1}{G_1} \\ \frac{G_1^2 - G_0^2}{G_1} & \frac{-G_0}{G_1} \end{pmatrix} \cdot \begin{pmatrix} 1 & 0 \\ G_{RF} & 1 \end{pmatrix} \tag{3-20}$$

$$= \begin{pmatrix} \frac{-G_0 - G_{RF}}{G_1} & \frac{-1}{G_1} \\ \frac{-G_0 \cdot (G_{IF} + G_{RF}) - G_{IF} \cdot G_{RF} - G_0^2 + G_1^2}{G_1} & \frac{-G_0 - G_{IF}}{G_1} \end{pmatrix}$$

The resulting Y parameters of the whole cascaded two port network is:

$$\begin{pmatrix} y_{11} & y_{12} \\ y_{21} & y_{22} \end{pmatrix} = \begin{pmatrix} \frac{D}{B} & \frac{A \cdot D - B \cdot C}{B} \\ \frac{-1}{B} & \frac{A}{B} \end{pmatrix} = \begin{pmatrix} G_0 + G_{IF} & G_1 \\ G_1 & G_0 + G_{RF} \end{pmatrix} \tag{3-21}$$

The transformation from Y parameters to Z parameters results in:

$$Z_{RF,g} = -\frac{y_{21}}{|y|} = -\frac{G_1}{(G_0+G_{IF})(G_0+G_{RF})-G_1^2} \tag{3-22}$$

Now the efficiency of the mixer can be determined from Eqn. (3-15) and Eqn. (3-22).

$$\eta = 4G_{IF}\cdot G_{RF}\cdot |Z_{RF,g}|^2 = 4G_{IF}\cdot G_{RF}\cdot \left| \frac{G_1}{(G_0+G_{IF})(G_0+G_{RF})-G_1^2} \right|^2 \tag{3-23}$$

Among these four parameters (G_{IF}, G_{RF}, G_0, and G_1), the source and load conductances are assumed to match the frequency selective networks in the analysis, that is, both G_{IF} and G_{RF} are 0.02S. G_0 and G_1 depend on Vb, V_{LO} and the nonlinearity of the RTD I-V curve. In reality V_{LO} is replaced by the LO power P_{LO}:

$$P_{LO} = \text{LO input power} = \left(\frac{V_{LO}}{\sqrt{2}}\right)^2 / R_{LO} = \frac{V_{LO}^2}{2R_{LO}}(W) \tag{3-24}$$

$$= 10\log\left(1000\cdot\frac{V_{LO}^2}{2R_{LO}}\right)(dBm) = 30+10\log\left(\frac{V_{LO}^2}{2R_{LO}}\right)(dBm)$$

Therefore, Vb, P_{LO} and the nonlinearity of the RTD I-V curve determine the power efficiency of the RTD mixer.

Letting the bias voltage Vb vary from -1 to 1V, P_{LO}=-19dBm, using Eqn. (3-23), the theoretical calculated power efficiency of the RTD mixer versus bias voltage Vb is shown below, with the overlaid I-V curve.

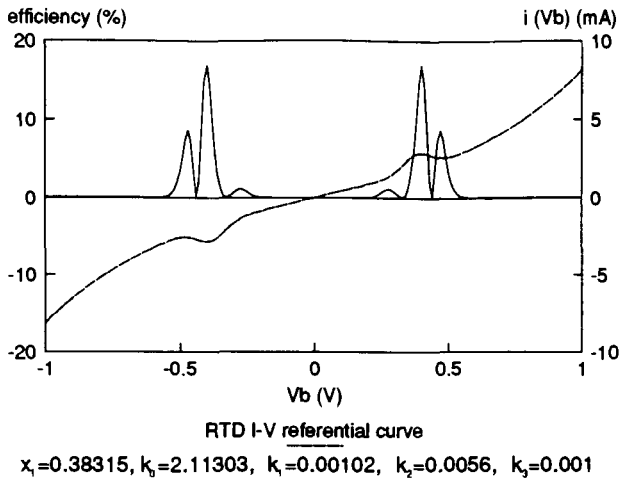

Fig. 3.6 Theoretical RTD mixer power efficiency versus bias voltage

The plot above shows that two peaks in the power efficiency of the RTD mixer occur at the peak and valley voltages (V_P, V_V), with the one occurring at V_P much higher than the other. Also, a minor peak in the power efficiency occurs before the NDR region, due to the small flexure in the RTD I-V curve model.

3.1.3 Theoretical Efficiency As A Function of the RTD Mixer Parameters

In the last section, the conclusion was drawn that Vb, P_{LO} and the nonlinearity of the RTD I-V curve determine the power efficiency of the RTD mixer, we can observe how these parameters affect the power efficiency of the RTD mixer. This will provide us with insight into how to optimize the RTD structure to maximize the efficiency of a mixer.

3.1.3.1 The effect of the nonlinearity of the RTD I-V curve

Since the physical meaning of x_1, k_0, k_1, k_2 and k_3 (k_3 is a constant) are known, one can change one of the four parameters (x_1=0.38315, k_0=2.11303, k_1=0.00102, k_2=0.0056) at one time and observe the power efficiency of the RTD mixer.

A) x_1 parameter

From the efficiency (versus Vb) curves and the referential RTD I-V curves plotted below, one can tell that since x_1 controls the position of the peak current point (V_P,I_P). When x_1 is increased, V_P and I_P are increased, G_P, G_D, and R_I are all decreased, and the power efficiency of the RTD mixer decreases.

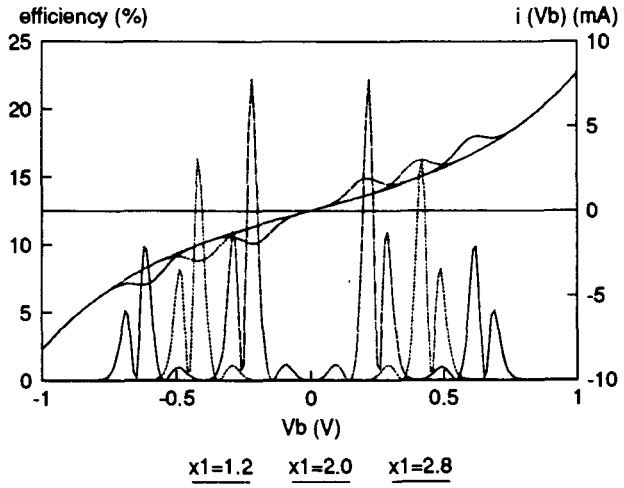

Fig. 3.7 Power efficiency of the RTD mixer with varying x_1 (P_{LO}=-19dBm)

B) k_0 parameter

From the efficiency (versus Vb) curves and the referential RTD I-V curves plotted below, one can tell that k_0 controls the slope of the RTD I-V curve. When k_0 is increased, G_P increases, but V_P, G_D and R_I all decrease, and the power efficiency of the RTD mixer decreases.

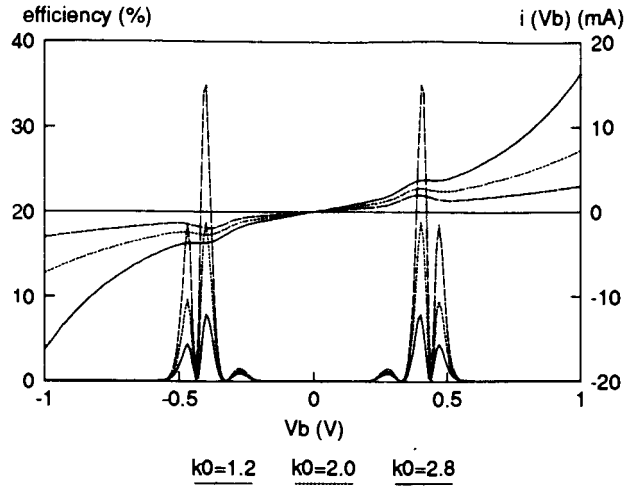

Fig. 3.8 Power efficiency of the RTD mixer with varying k_0 (P_{LO}=-19dBm)

C) k_1 parameter

From the efficiency (versus Vb) curves and the referential RTD I-V curves plotted below, one can tell that k_1 controls the peak current value I_P. When k_1 is increased, V_P, V_V and I_V remain unchanged, meanwhile G_P, G_D and R_I are all increased, and the power efficiency of the RTD mixer increases.

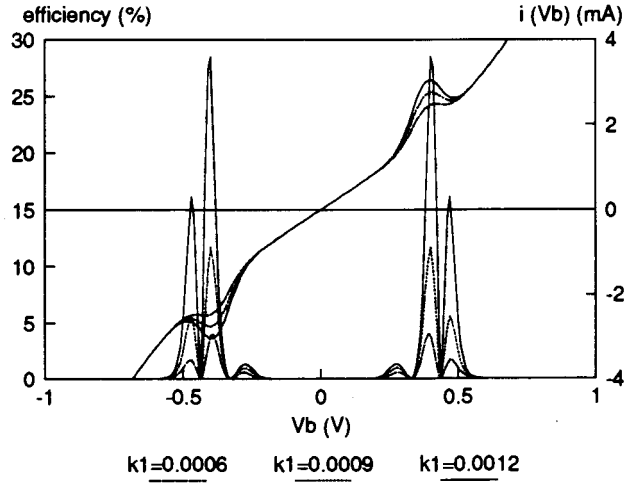

Fig. 3.9 Power efficiency of the RTD mixer with varying k_1 (P_{LO}=-19dBm)

D) k_2 parameter

From the efficiency (versus Vb) curves and the referential RTD I-V curves plotted below, one can tell that one can tell that k_2 controls the position of the valley current point (V_V, I_V). When k_2 is increased, the peak current point (V_P, I_P) stays in the same position, while the valley current point drifts along the original I-V curve. G_P will stay the same value, G_D and I_R decrease, and the power efficiency of the RTD mixer decreases.

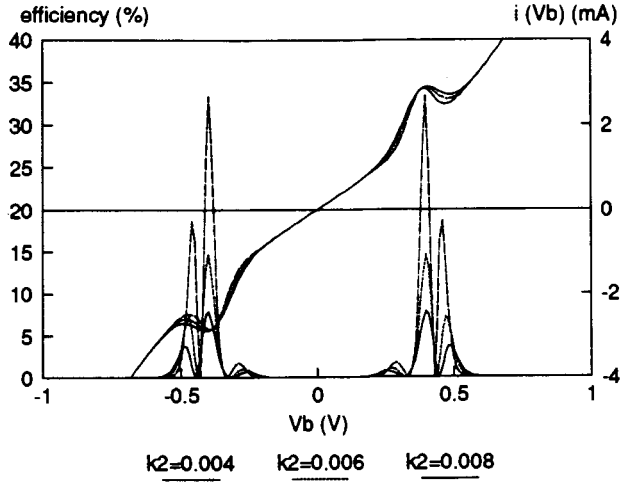

Fig. 3.10 Power efficiency of the RTD mixer with varying k_2 (P_{LO}=-19dBm)

From the four plots above, one can draw the conclusion that the power efficiency of the RTD mixer is an increasing function of G_D and I_R.

3.1.3.2 The effect of varying the bias voltage Vb and the LO power P_{LO}

A) Efficiency of the RTD mixer versus P_{LO} with different Vb values

Varying P_{LO} from -30 to 0 dBm, while Vb=0.35, 0.4 and 0.5V respectively, the efficiency plot of the RTD mixer is shown below:

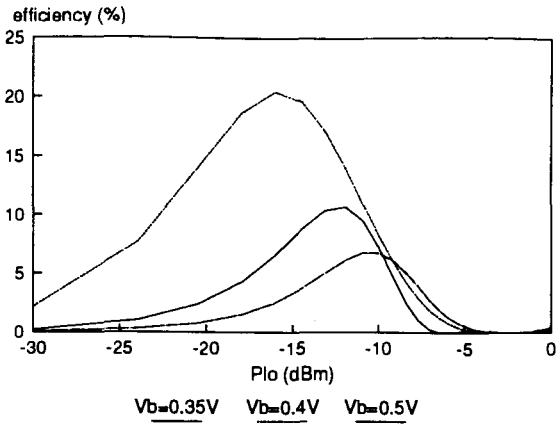

Fig. 3.11 Power efficiency of the RTD mixer versus P_{LO} when Vb=0.35, 0.4 and 0.5V

The plot above shows that 1) the power efficiency of the RTD mixer increases until the optimum LO drive level is reached, and then decreases, as the mixer compresses at high LO drive levels; 2) For a different RTD DC bias voltage, the optimum LO drive level varies, as does the overall power efficiency of the RTD mixer.

B) Efficiency of the RTD mixer versus Vb with different P_{LO} values

Varying Vb from -1 to 1V, while P_{LO}=-20.5, -15.9 and -11.9dBm respectively, the power efficiency of the RTD mixer is shown below:

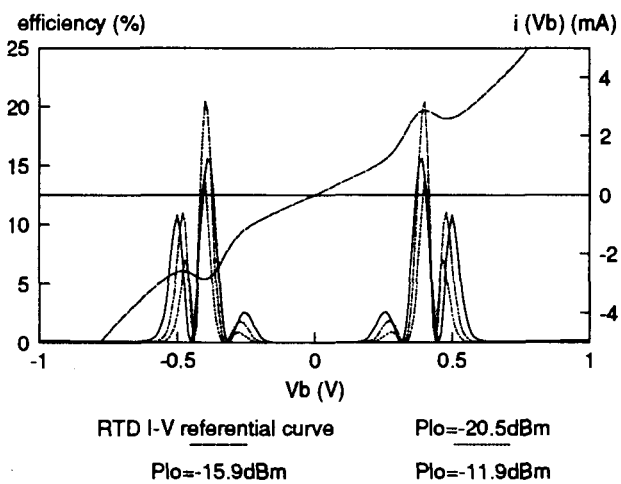

Fig. 3.12 Power efficiency of the RTD mixer versus Vb when P_{LO}=-20.5, -15.9 and -11.9dBm

The plot above shows that 1) two peaks in the power efficiency of the RTD mixer occur at the peak and valley voltages (V_P, V_V), with the one occurring at V_P much higher than the other. Also, a minor peak in the power efficiency occurs before the NDR region, due to the small flexure in the RTD I-V curve model; 2) For a different P_{LO}, the overall power efficiency of the RTD mixer changes, too.

3.2 RTD Multiplier

3.2.1 RTD Multiplier Configuration

To obtain the efficiency of an RTD multiplier, the multiplier topology needs to be specified. The configuration of the multiplier is shown in Fig. 3.13. Vb is the DC bias voltage, and R_{IF} and R_{RF} are the source and load impedances, respectively. Vg is the voltage source. The two band pass filters BPF_IF, BPF_RF are frequency selective networks, whose impedances are zero at f_{IF}, f_{RF}, respectively, and infinite at all other frequencies. Thus the only voltages which can exist across the diode are the DC bias voltage Vb, V_{IF} at the IF frequency f_{IF}, and V_{RF} at the RF frequency f_{RF}.

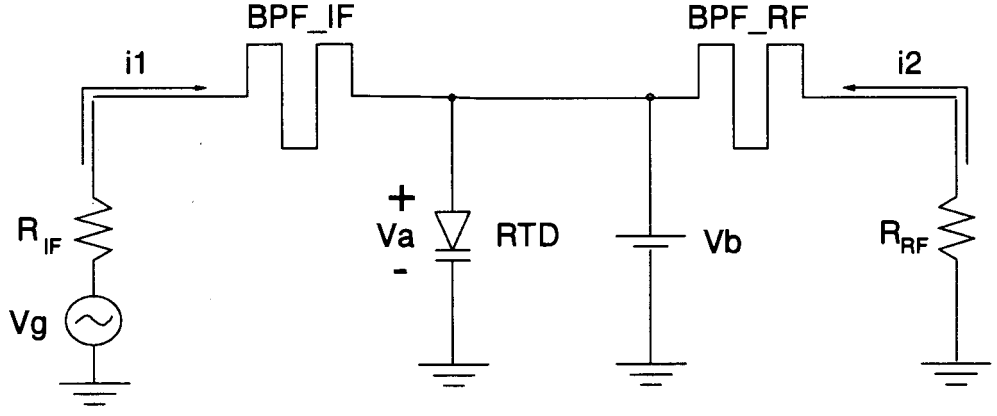

Fig. 3.13 Configuration of the RTD multiplier showing the IF and RF ports

3.2.2 RTD Multiplier Efficiency

The efficiency of a multiplier is the ratio of the load power at the RF port to the power available from the IF source. As illustrated in Fig. 3.13, assuming the corresponding ac voltage at the RTD is Va when the voltage source Vg is applied at the IF port. When the RTD is biased at a bias voltage Vb, the current of the RTD can be expressed as a Fourier series:

$$\begin{aligned} i_{RTD}(\theta) &= i(Vb + Va \cdot \cos\theta) \\ &= k_3 \cdot \left(e^{k_0 \cdot (Vb + Va \cdot \cos\theta)} - e^{-k_0 \cdot (Vb + Va \cdot \cos\theta)} \right) \\ &\quad + k_1 \cdot \left[e^{-\frac{(Vb + Va \cdot \cos\theta - x_1)^2}{k_2}} - e^{-\frac{(Vb + Va \cdot \cos\theta + x_1)^2}{k_2}} \right] \\ &= i_0 + i_1 \cdot \cos\theta + i_2 \cdot \cos 2\theta + \cdots \end{aligned} \tag{3-25}$$

Where

$$\theta = \omega_0 \cdot t \tag{3-26}$$

$$i_0 = \frac{1}{2\pi}\int_{-\pi}^{\pi} i_{RTD}(\theta)d\theta = \frac{1}{\pi}\int_0^{\pi} i_{RTD}(\theta)d\theta \tag{3-27}$$

$$i_1 = \frac{1}{\pi}\int_{-\pi}^{\pi} i_{RTD}(\theta)\cdot\cos\theta d\theta = \frac{2}{\pi}\int_0^{\pi} i_{RTD}(\theta)\cdot\cos\theta d\theta \tag{3-28}$$

$$i_2 = \frac{1}{\pi}\int_{-\pi}^{\pi} i_{RTD}(\theta)\cdot\cos(2\theta) d\theta = \frac{2}{\pi}\int_0^{\pi} i_{RTD}(\theta)\cdot\cos(2\theta) d\theta \tag{3-29}$$

i_0 is the DC current of RTD, i_1 and i_2 are the first and second current harmonics of RTD, respectively, i_3 and higher order terms are neglected, as they produce signals at frequencies other than the frequencies f_{IF} and f_{RF}, and the higher order harmonic products are assumed to be open-circuited.

The relationship between Va and Vg can be expressed as

$$Va = Vg - i_1 \cdot R_{IF} \tag{3-30}$$

To make the analysis analytically tractable, Va is assumed to be constant versus Vb, which means that Vg will no longer be a constant any more. However, this assumption won't change the analytical power efficiency of the RTD multiplier which is the power ratio between the RF and IF ports, as Va is only an intermediate variable. With the current coefficients (i_1, i_2) given above, the input and output power can be formulated.

$$P_{OUT} = \text{load power at } f_{RF} = \frac{1}{T}\int_0^T [i_2 \cdot \cos(2\omega_0 t)]^2 \cdot R_{RF} dt = \frac{i_2^2 \cdot R_{RF}}{2} \tag{3-31}$$

$$P_{IN} = \text{power available from IF source at } f_{IF} \tag{3-32}$$

$$= \left(\frac{1}{2}\frac{V_g}{\sqrt{2}}\right)^2 / R_{IF} = \frac{(i_1 \cdot R_{IF} + Va)^2}{8R_{IF}}$$

Thus the expression for the power efficiency of the RTD multiplier is obtained:

$$\eta = \frac{P_{OUT}}{P_{IN}} = \frac{4i_2^2 \cdot R_{RF} \cdot R_{IF}}{(i_1 \cdot R_{IF} + Va)^2} \tag{3-33}$$

Among these five parameters (R_{IF}, R_{RF}, i_1, i_2 and Va), the source and load impedances are assumed to match the frequency selective networks in the analysis, that is, both R_{IF} and R_{RF} are 50ohm. i_1 and i_2 depend on Vb, Va and the nonlinearity of the RTD I-V curve. Since Va is just an intermediate

variable, one would be more interested in its activating voltage - the IF input voltage source Vg or the IF input power P_{IN}. From Eqn. (3-30) one can tell that Va can be replaced by Vg or P_{IN} (here P_{IN} is chosen). Therefore, Vb, P_{IN} and the nonlinearity of the RTD I-V curve determine the power efficiency of the RTD multiplier.

Letting the bias voltage Vb vary from -1 to 1V, Va=0.075V, using equation (3-33), the theoretical calculated power efficiency of the RTD multiplier versus bias voltage Vb is shown below, with the overlaid I-V curve:

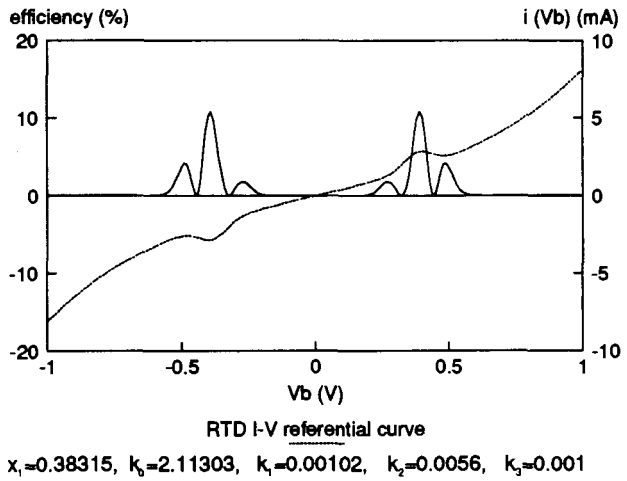

Fig. 3.14 Theoretical RTD multiplier power efficiency versus bias voltage

The plot above shows that two peaks in the power efficiency of the RTD multiplier occur at the peak and valley voltages (V_P, V_V), with the one occurring at V_P much higher than the other. Also, a minor peak in the power efficiency occurs before the NDR region, due to the small flexure in the RTD I-V curve model.

3.2.3 Theoretical Efficiency As A Function of RTD Multiplier Parameters

In the last section, the conclusion was drawn that Vb, P_{IN} and the nonlinearity of RTD I-V curve determine the power efficiency of the RTD multiplier, we can now observe how these parameters affect the power efficiency of the RTD multiplier.

3.2.3.1 The effect of the nonlinearity of the RTD I-V curve

Since the physical meaning of x_1, k_0, k_1, k_2 and k_3 (k_3 is a constant) are known, one can change one of the four parameters (x_1=0.38315, k_0=2.11303, k_1=0.00102, k_2=0.0056) at a time and observe the power efficiency of the RTD multiplier.

A) x_1 parameter

From the efficiency (versus Vb) curves and the referential RTD I-V curves plotted below, one can tell that since x_1 controls the position of the peak current point (V_P,I_P). When x_1 is increased, V_P and I_P are increased, G_P, G_D, and R_I are all decreased, and the power efficiency of the RTD multiplier decreases.

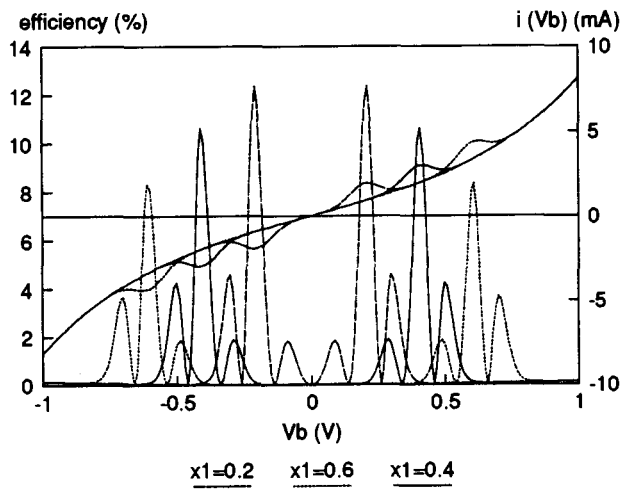

Fig. 3.15 Power efficiency of the RTD multiplier with varying x_1 (Va=0.075V)

B) k_0 parameter

From the efficiency (versus Vb) curves and the referential RTD I-V curves plotted below, one can tell that k_0 controls the slope of the RTD I-V curve. When k_0 is increased, G_P increases, but V_P, G_D and R_I all decrease, and the power efficiency of the RTD multiplier decreases.

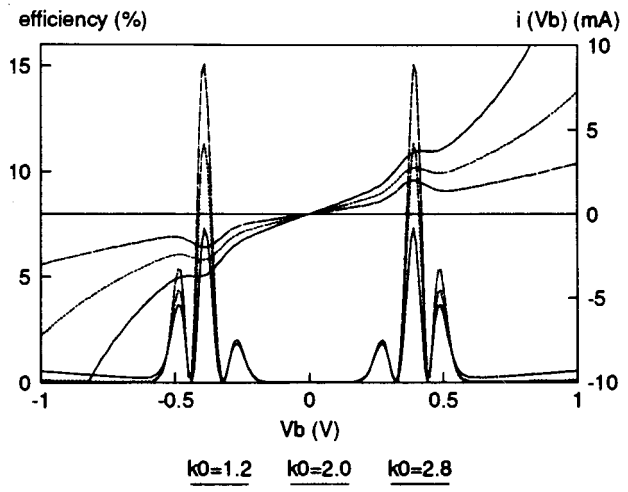

Fig. 3.16 Power efficiency of the RTD multiplier with varying k_0 (Va=0.075V)

C) k_1 parameter

From the efficiency (versus Vb) curves and the referential RTD I-V curves plotted below, one can tell that k_1 controls the peak current value I_P. When k_1 is increased, V_P, V_V and I_V remain unchanged, meanwhile G_P, G_D and R_I are all increased, and the power efficiency of the RTD multiplier increases.

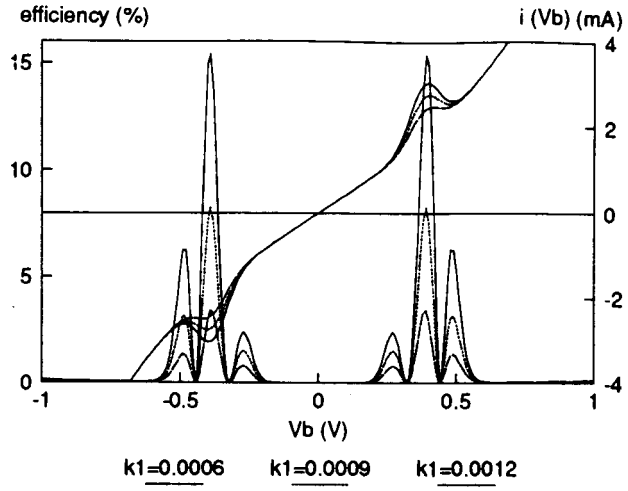

Fig. 3.17 Power efficiency of the RTD multiplier with varying k_1 (Va=0.075V)

D) k_2 parameter

From the efficiency (versus Vb) curves and the referential RTD I-V curves plotted below, one can tell that one can tell that k_2 controls the position of the valley current point (V_V, I_V). When k_2 is increased, the peak current point (V_P, I_P) stays in the same position, while the valley current point drifts along the original I-V curve. G_P will stay the same value, G_D and I_R decrease, and the power efficiency of the RTD multiplier decreases.

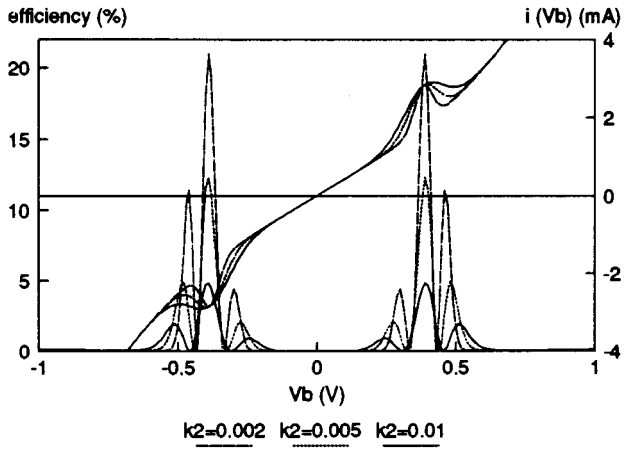

Fig. 3.18 Power efficiency of the RTD multiplier with varying k_2 (Va=0.075V)

From the four plots above, one can draw the conclusion that the power efficiency of the RTD multiplier is an increasing function of G_D and I_R.

3.2.3.2 The effect of varying the bias voltage Vb and the IF input power

A) Efficiency of the RTD multiplier versus P_{IN} with different Vb values

To get the relationship between the power efficiency of the RTD multiplier and P_{IN}, the intermediate parameter Va will be functioned as a bridge. Varying Va from 0.01 to 0.15V, two data sets (the power efficiency of the RTD multiplier and P_{IN}) are obtained, leaving P_{IN} in the x-axis and the power efficiency of the RTD multiplier in the y-axis, while Vb=0.3, 0.4 and 0.5 respectively, the plot is shown below:

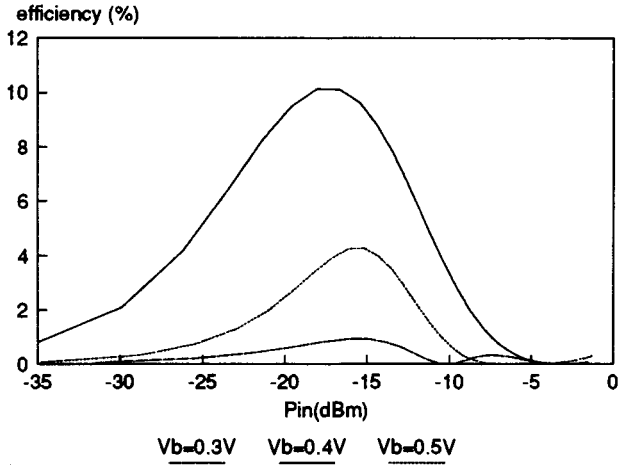

Fig. 3.19 Power efficiency of the RTD multiplier versus P_{IN} when Vb=0.3, 0.4 and 0.5V

The plot above shows that 1) the power efficiency of the RTD multiplier increases until the optimum P_{IN} level is reached, and then decreases as the multiplier compresses at high P_{IN} levels, 2) For a different RTD DC bias voltage, the optimum P_{IN} level varies, as does the overall power efficiency of the RTD multiplier.

B) Efficiency of the RTD multiplier versus Vb with different P_{IN} values

To obtain the relationship between the power efficiency of the RTD multiplier and Vb (with different P_{IN} values), the intermediate parameter Va will be used as a bridge. First of all, one needs to find the relationship between P_{IN} and Va. Using Eqn. (3-30) and (3-32), plot of Vg and the input power P_{IN} versus Va is shown below:

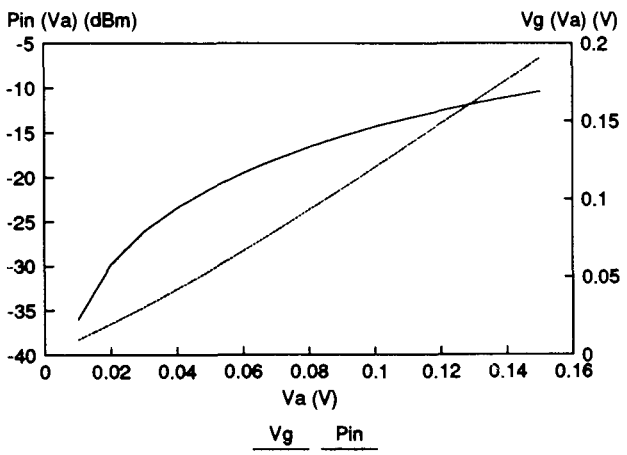

Fig. 3.20 Vg and the input power P_{IN} versus Va (Vb=0.4V)

The plot above shows that both Vg and P_{IN} are increasing functions of Va. Therefore to obtain the power efficiency of the RTD multiplier versus Vb with different P_{IN} values, one needs only to determine the power efficiency of the RTD multiplier versus Vb with different Va values.

Varying Vb from -1 to 1V, while Va=0.04, 0.075 and 0.1V respectively, the following plot shows the power efficiency of the RTD multiplier versus Vb with different P_{IN} values and a overlaid I-V curve:

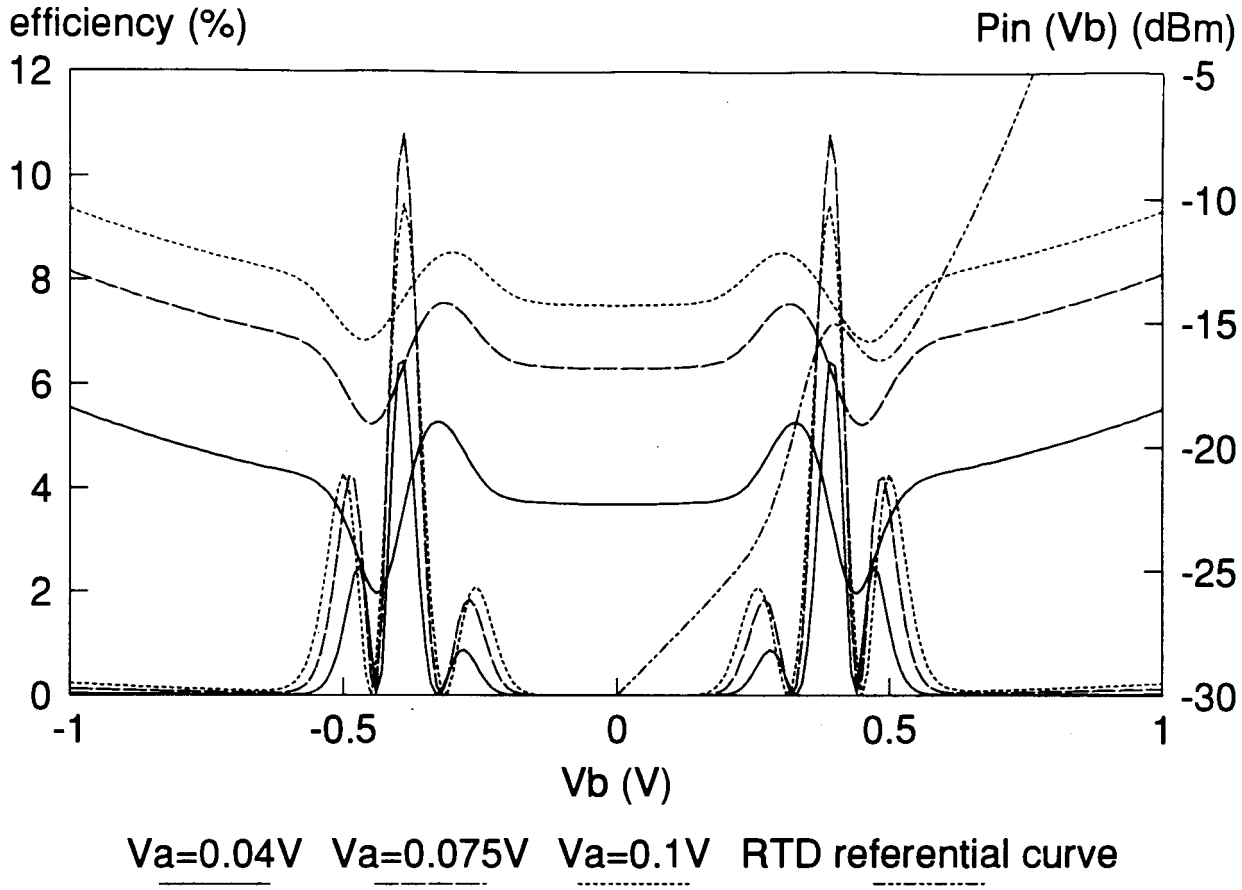

Fig. 3.21 Power efficiency of the RTD multiplier and the input power P_{IN} versus Vb when Va=0.04, 0.075 and 0.1V

The plot above shows that 1) two peaks in the power efficiency of the RTD multiplier occur at the peak and valley voltages (V_P, V_V), with the one occurring at V_P much higher than the other. Also, a minor peak in the power efficiency occurs before the NDR region, due to the small flexure in the RTD I-V curve model; 2) For a different P_{IN}, the overall power efficiency of the RTD multiplier changes, too.

4 DESIGN OF RTD MIXER AND MULTIPLIER

In chapter 3, the theoretical calculations about the performance of RTD mixer and multiplier assume that the source and load impedances are matched and that optimum reactive loads at all idler frequencies are realized. In reality the circuits were made using microstrip transmission lines, therefore a number of parameters need to be considered, such as impedance matching, dielectric constant of the substrate, attenuation of the microstrip line, etc. To account for these parameters, a powerful microwave simulation package ACADEMY is required to aid the circuit design.

4.1 RTD Mixer

The simple sketch of the RTD mixer is shown in Fig. 4.1. A, B and C are matching transmission lines between the RTD and the three filters. Instead of a bandpass filter (BPF), a lowpass filter (LPF) is chosen to be the IF port frequency selective network for two reasons: 1) the size of a LPF is much smaller than that of a BPF with the same stop frequency, 2) most of the BPFs tend to have a spurious pass-band at their second harmonic, while for the LPFs the pass-band occurs at their fourth harmonic. The IF input frequency is 3GHz, LO frequency 11GHz, and RF output frequency 14GHz.

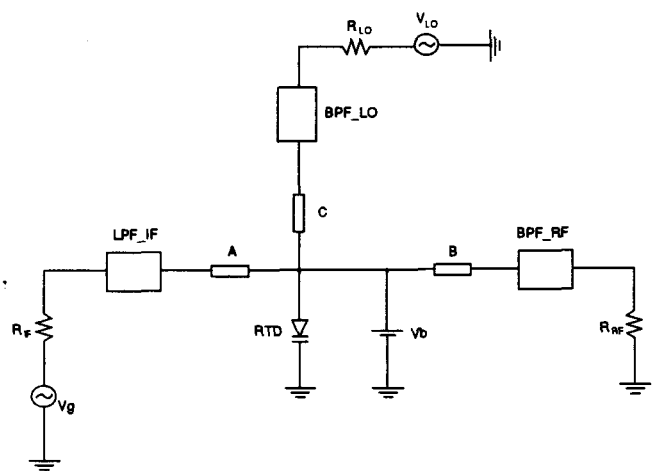

Fig. 4.1 Simple sketch of the RTD mixer

4.1.1 Principles of IF LPF Design for the RTD Mixer

Considering the frequency existing in each port, the IF LPF for the mixer should be able to let the signals with frequencies around 3GHz or less pass through, and filter out the signals with frequencies around 11GHz or higher. Thus the pass-band edge frequency f1 is chosen to be 6GHz, and the stop-band frequency f' is chosen to be 11 GHz.

According to the requirement of the pass-band attenuation and the stop-band attenuation, one can find the minimum number of reactive elements n in the filter [30].

$$n \geq \frac{acosh\left(\sqrt{\frac{10^{\frac{L'ar}{10}}-1}{10^{\frac{Lar}{10}}-1}}\right)}{acosh\left(\frac{\omega'}{\omega 1}\right)} \qquad (4\text{-}1)$$

where

Lar..... The maximum dB attenuation in the pass band.
ω1 ..... The equal-ripple pass band edge frequency.
ω' ..... A frequency in the stop band.
L'ar ..... The dB attenuation corresponding to ω'

Let Lar=0.01dB, $\omega 1 = 2\pi f1 = 12\pi(Grad/s)$, L'ar=55dB and $\omega' = 2\pi f' = 22\pi(Grad/s)$, one can get n=8.2819. To get a symmetrical structure, n needs to be odd, so n=9 is chosen for the LPF.

Given two different characteristic impedances (Z_h=77ohm, Z_l=27ohm) for the transmission lines of the LPF, through the procedure described in the filter design handbooks [31, 32, 33], the electrical length of each transmission line of the IF LPF can be obtained. The in-band and wide band attenuation plots are shown below:

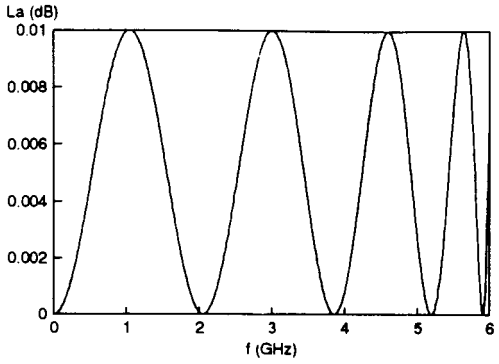

Fig. 4.2 Theoretical result of inband LPF of the mixer

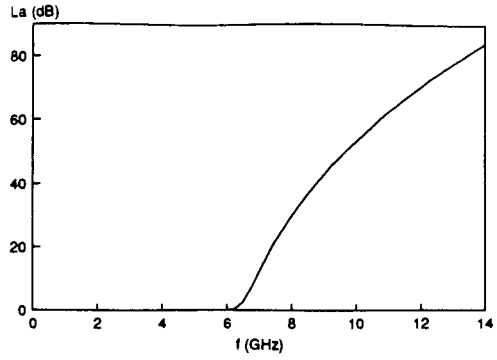

Fig. 4.3 Theoretical result of wide band LPF of the mixer

4.1.2 Principles of RF BPF Design for the RTD Mixer

Considering the frequency existing in each port, the RF BPF for the mixer should be able to let the signals with frequencies around 14GHz pass through, and it's attenuation should be high at frequencies round 11GHz and 3 GHz. Thus the pass-band center frequency f0 is chosen to be 14GHz, the equal edge-ripple pass band edge frequencies are chosen to be f1=13.3GHz and f2=14.7GHz, so that the fractional bandwidth $w=(f_2-f_1)/f_0=0.1$, and the stop-band frequency f' is chosen to be 9 GHz.

According to the requirement of the pass-band attenuation and the stop-band attenuation, one can find the minimum number of reactive elements n in the filter.

$$n \geq \frac{acosh\left(\sqrt{\frac{10^{\frac{L'ar}{10}}-1}{10^{\frac{Lar}{10}}-1}}\right)}{acosh\left(2\left|\frac{\omega'-\omega 0}{\omega 2-\omega 1}\right|\right)} \qquad (4\text{-}2)$$

where

$\omega 0$ ..... Pass band center frequency.
Lar..... The maximum dB attenuation in the pass band.
$\omega 1$, $\omega 2$ ..... The equal-ripple pass band edge frequencies.
ω' ..... A frequency in the stop band.
L'ar ..... The dB attenuation corresponding to ω'

Let Lar=0.01dB, $\omega 1 = 2\pi f1 = 2\pi 13.3 = 26.6\pi(Grad/s)$, $\omega 2 = 2\pi f2 = 2\pi 14.7 = 29.4\pi(Grad/s)$, L'ar=55dB and $\omega' = 2\pi f' = 2\pi 9 = 18\pi(Grad/s)$, one can get n=3.7906. Since the structure of a bandpass filter is always symmetrical, n=4 is chosen for the RF BPF of the mixer.

With a 50ohm characteristic impedance transmission line terminating at each end of the RF BPF, through the procedure described in the filter design handbooks [31, 32, 33], the even-and odd-mode impedance of each transmission line of the RF BPF can be obtained. The in-band and wide band attenuation plots are shown below:

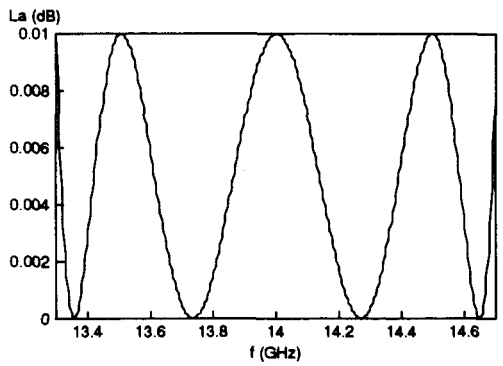

Fig. 4.4 Theoretical result of inband RF BPF of the mixer

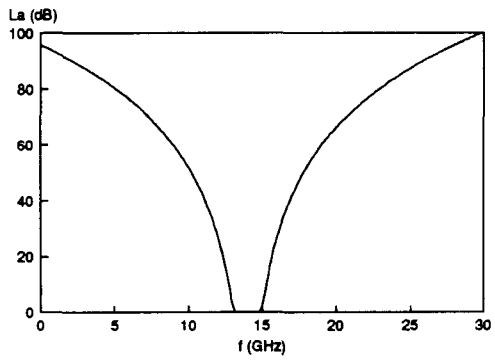

Fig. 4.5 Theoretical result of wide band RF BPF of the mixer

4.1.3 Principles of LO BPF Design for the RTD Mixer

Considering the frequency existing in each port, the LO BPF for the mixer should be able to let the signals with frequencies around 11GHz pass through, and it's attenuation should be high at frequencies round 14GHz and 3 GHz. Thus the pass-band center frequency f0 is chosen to be 11GHz,

the equal edge-ripple pass band edge frequencies are chosen to be f1=10.45GHz and f2=11.55GHz, so that the fractional bandwidth $w=(f_2-f_1)/f_0=0.1$, and the stop-band frequency f' is chosen to be 14 GHz.

According to the requirement of the pass-band attenuation and the stop-band attenuation, one can find the minimum number of reactive elements n in the filter through Eqn. (4-2).

Let Lar=0.1dB, $\omega 1 = 2\pi f1 = 2\pi 10.45 = 20.9\pi(Grad/s)$, $\omega 2 = 2\pi f2 = 2\pi 11.55 = 23.1\pi(Grad/s)$, L'ar=55dB and $\omega' = 2\pi f' = 2\pi 14 = 28\pi(Grad/s)$, one can get n=3.7399. Since the structure of a bandpass filter is always symmetrical, n=4 is chosen for the LO BPF of the mixer.

Through the same procedure as described in section 4.1.2, the even-and odd-mode impedance of each transmission line can be obtained. The in-band and wide band attenuation plots are shown below:

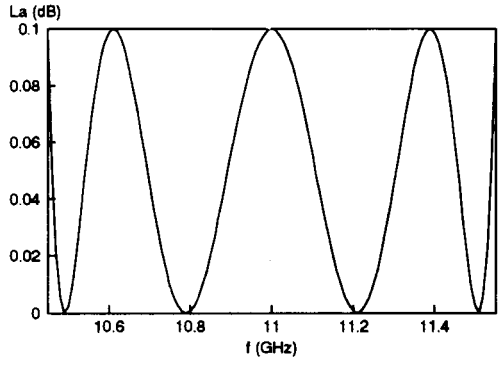

Fig. 4.6 Theoretical result of inband LO BPF of the mixer

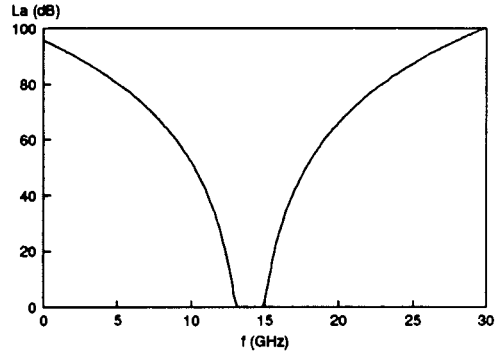

Fig. 4.7 Theoretical result of wide band LO BPF of the mixer

4.1.4 Simulation of the Three Filters of the RTD mixer

After the data (even- and odd-mode impedances of BPF, the characteristic impedances and electrical lengths of LPF) were obtained from the principle design, they were input to a parameter transfer

package LineCalc to be transferred to transmission lines' geometric parameters (lengths and widths). By varying the length and width of each microstrip line of the filters, the optimized results can be obtained in ACADEMY. The optimized results are shown below:

A) IF LPF of the mixer

The ACADEMY schematic of the IF LPF for the mixer is shown in Fig. 4.8, and the optimized simulation results of the mixer's IF LPF attenuation vs. frequency are shown in Fig. 4.9 and Fig. 4.10.

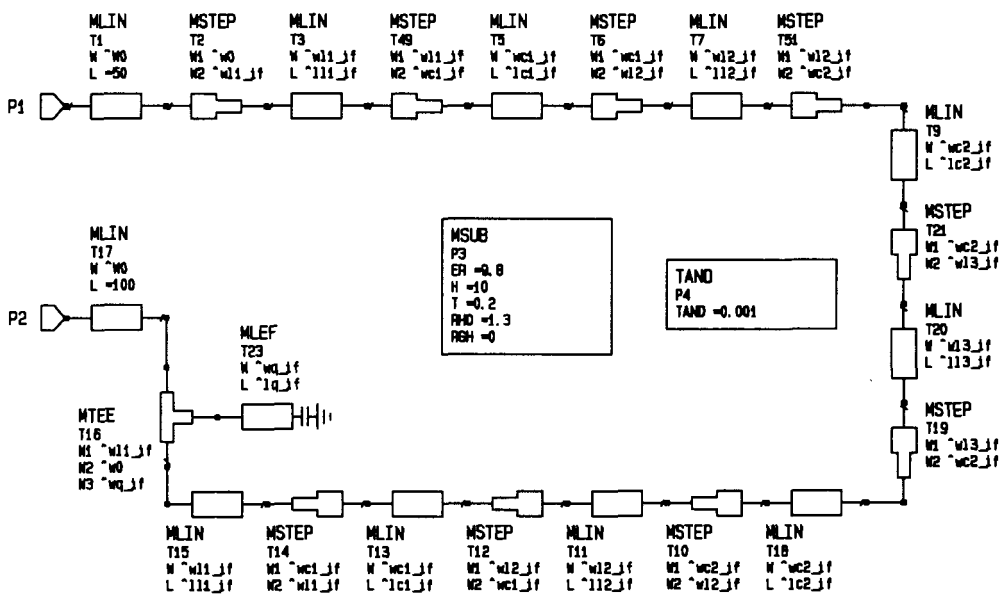

Fig. 4.8 ACADEMY schematic of the LPF for the mixer

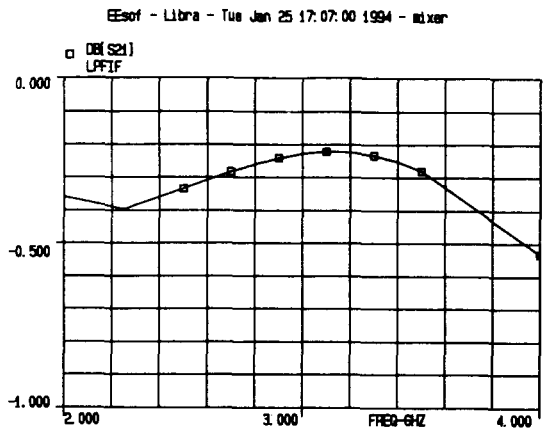

Fig. 4.9 Inband simulation result of the LPF of the mixer

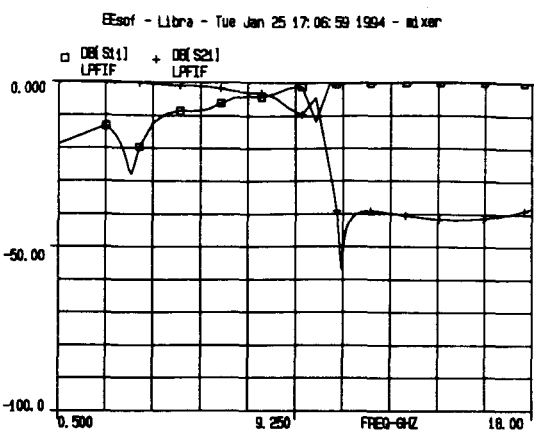

Fig. 4.10 Wide band simulation results of the LPF of the mixer

B) RF BPF of the mixer

The ACADEMY schematic of the RF BPF for the mixer is shown in Fig. 4.13, and the optimized simulation results of the mixer's RF BPF attenuation vs. frequency are shown in Fig. 4.11 and Fig. 4.12.

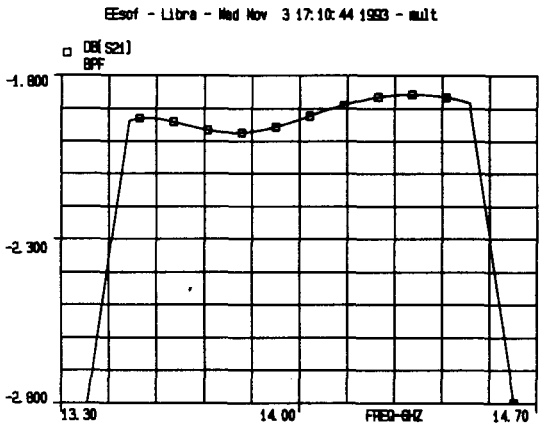

Fig. 4.11 Inband simulation result of the RF BPF of the mixer

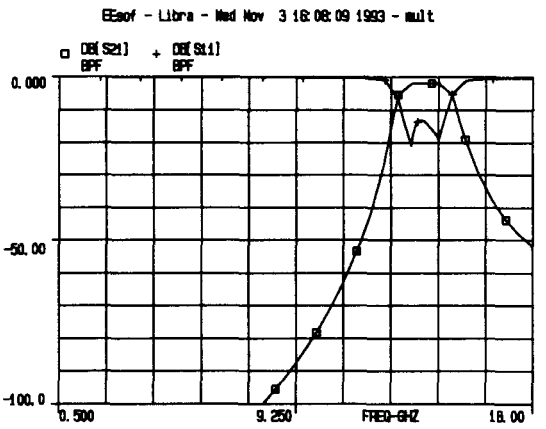

Fig. 4.12 Wide band simulation results of the RF BPF of the mixer

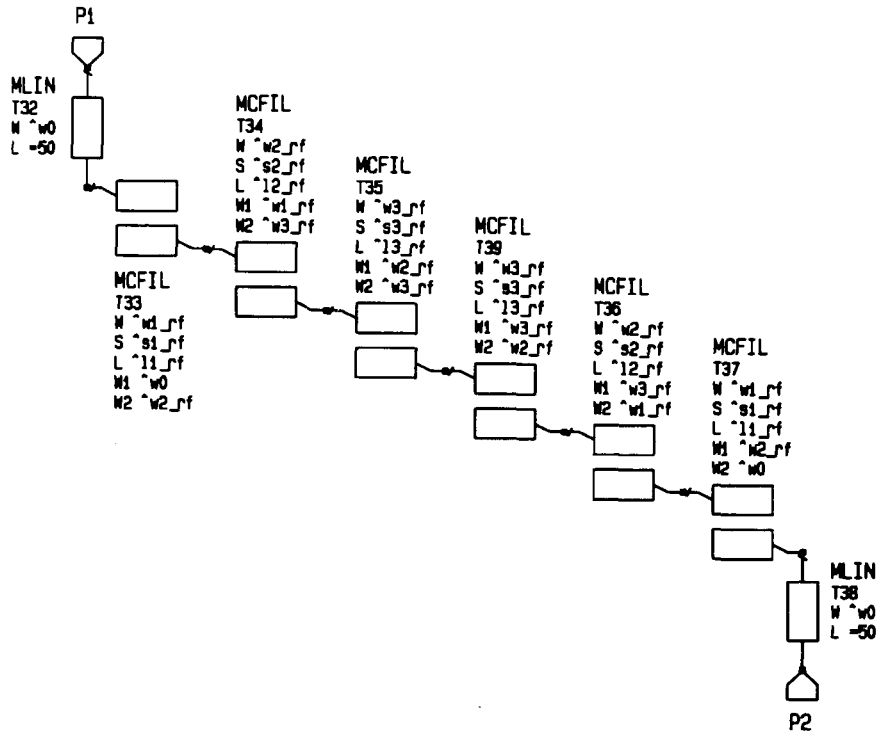

Fig. 4.13 ACADEMY schematic of the RF BPF for the mixer

C) LO BPF of the mixer

The ACADEMY schematic of the LO BPF for the mixer is similar to that of the RF BPF of the mixer. The optimized simulation results of the mixer's LO BPF attenuation vs. frequency are shown below:

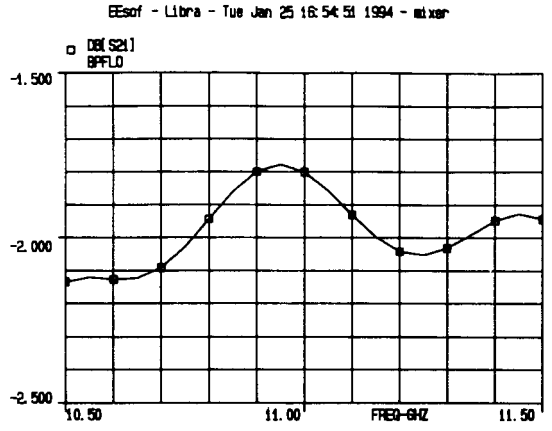

Fig. 4.14 Inband simulation result of the LO BPF of the mixer

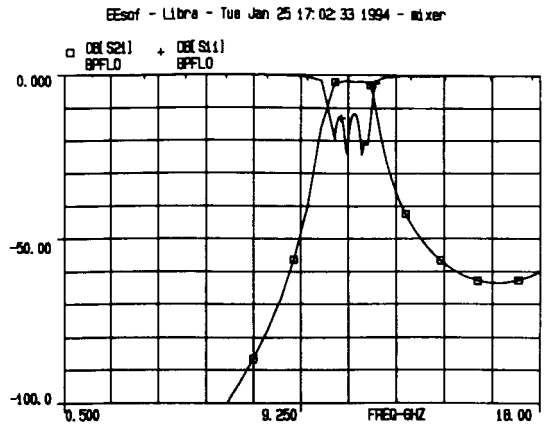

Fig. 4.15 Wide band simulation results of the LO BPF of the mixer

4.1.5 Simulation of the Other Circuit Components of the RTD Mixer

A) RTD I-V curve

The ACADEMY schematic model of the RTD is shown below:

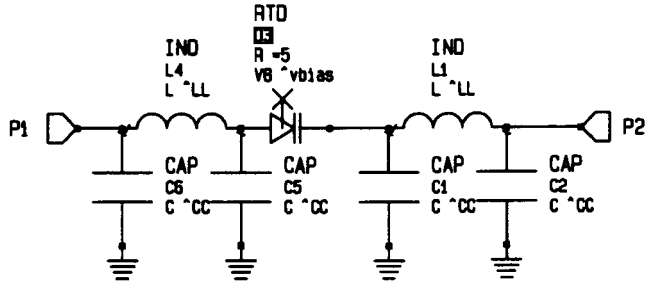

Fig. 4.16 ACADEMY schematic of the RTD

After storing a set of measured RTD I-V curve data into a C program, one can compile the C program into LIBRA to create a RTD model for ACADEMY. The simulation DC I-V curve of the RTD is obtained and can be subsequently be used in the simulations.

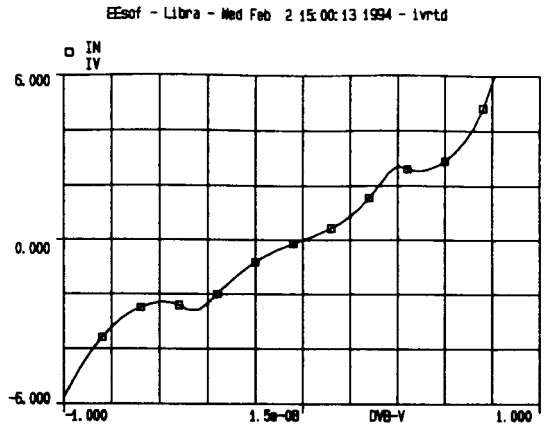

Fig. 4.17 Simulation DC I-V curve of the RTD

B) Bias block

The optimized simulation result of the DC bias of the mixer is shown below:

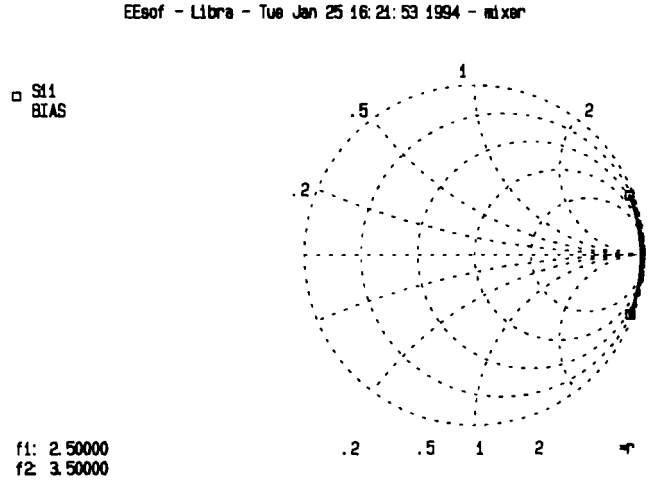

Fig. 4.18 Simulated S11 of the RTD mixer bias lock

The ACADEMY schematic of the bias block of the mixer is shown below:

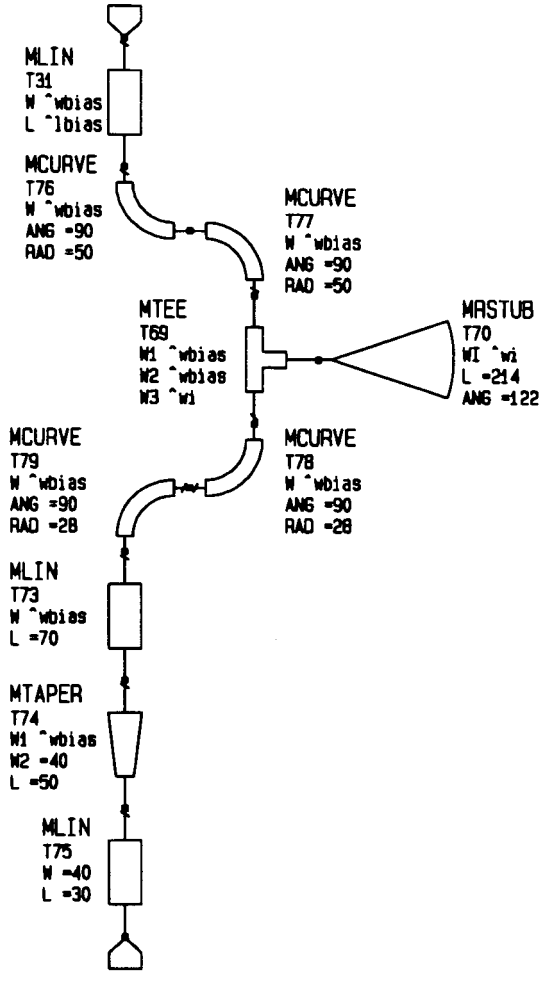

Fig. 4.19 ACADEMY schematic of the bias block of the mixer

4.1.6 Simulation of the Mixer

The individual blocks can be cascaded together forming the complete mixer.

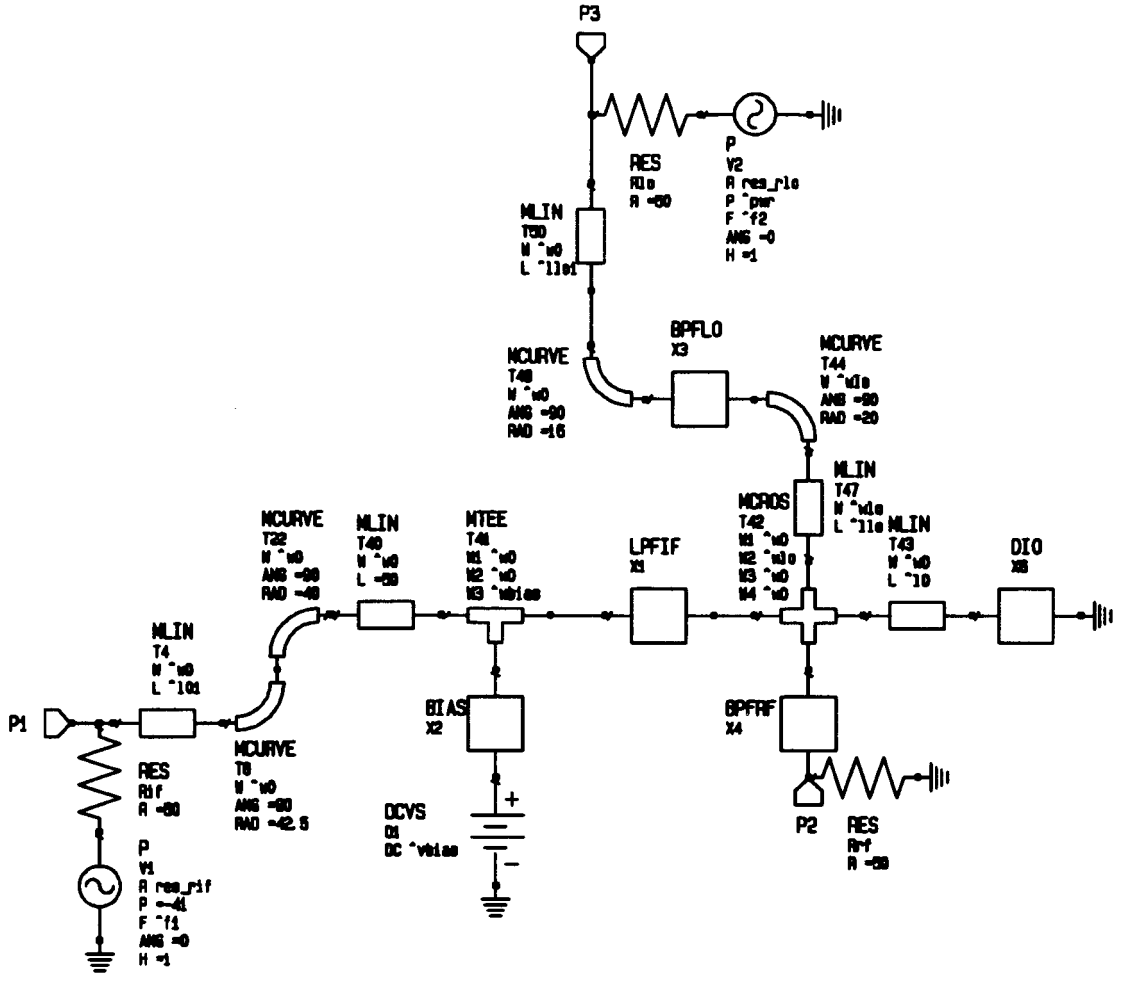

Fig. 4.20 ACADEMY schematic of the RTD mixer

It was found that by varying the lengths and widths of the three matching transmission lines, the power efficiency of the RTD mixer can change significantly. The final optimized simulation results of the RTD mixer are shown below:

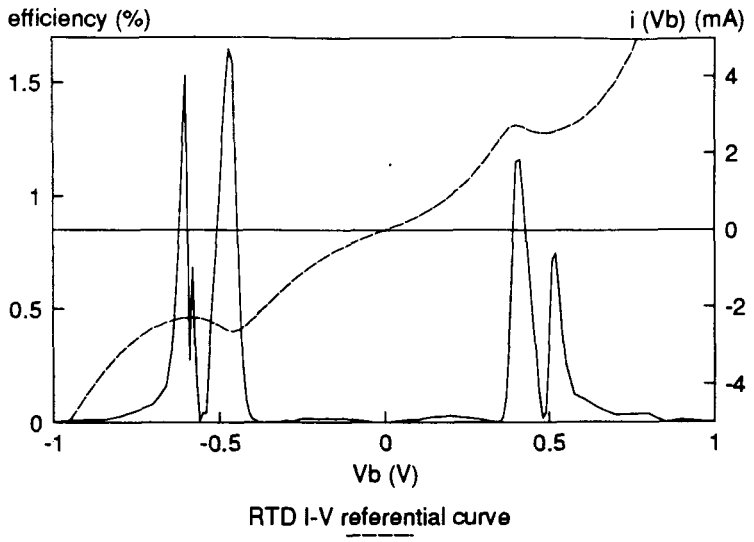

Fig. 4.21 Simulation power efficiency of the RTD mixer vs. bias voltage.

Compared to the theoretical result shown in Fig. 3.6, the plot above shows that two peaks in the power efficiency of the RTD mixer occur at the peak and valley voltages (V_P, V_V), with the one occurring at V_P much higher than the other. Also, a minor peak in the power efficiency occurs before the NDR region, due to the small flexure in the RTD I-V curve model. However, the negative part is not symmetrical to the positive part due to the asymmetry of the RTD I-V curve in simulation.

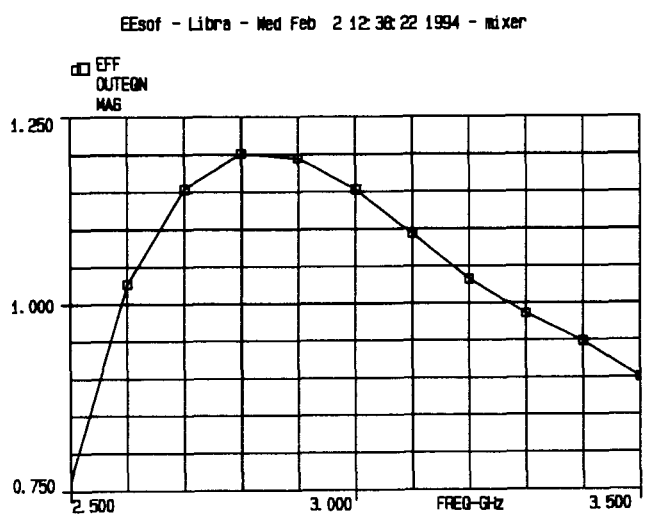

Fig. 4.22 Simulation power efficiency of the RTD mixer vs. inband frequency

The plot above shows that within the inband frequency, the RTD mixer obtained a maximum efficiency of 1.2% at the input frequency of 2.8GHz.

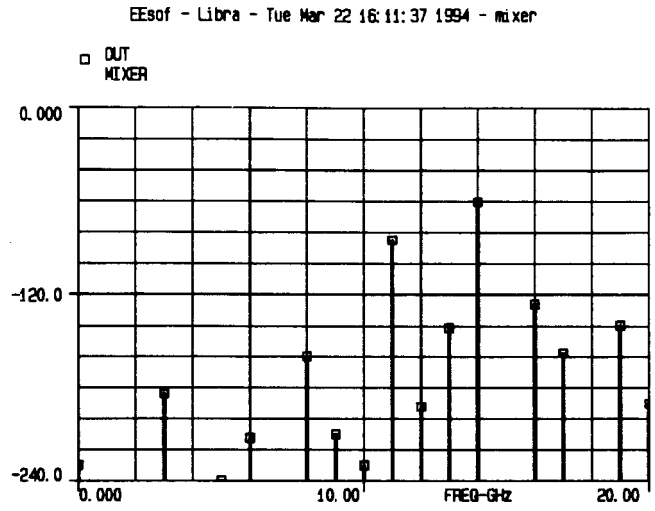

Fig. 4.23 Simulation power spectrum density of RTD mixer vs. wide band frequency

When the two sinusoidal frequencies (f_{IF} and f_{LO}) are applied to a mixer, the output signal of the mixer will contain frequency components at DC, f_{IF}, f_{LO}, $2f_{IF}$, $2f_{LO}$, $3f_{IF}$, $3f_{LO}$, $f_{IF} \pm f_{LO}$, $2f_{IF} \pm f_{LO}$, and $2f_{LO} \pm f_{IF}$, etc. Fig. 4.23 shows that, the input signal at f_{IF}=3GHz and LO signal at f_{LO}=11GHz are mixed by means of nonlinearities and switching to produce a group of signals having frequency components at DC, 3GHz (f_{IF}), 11GHz (f_{LO}), 6GHz ($2f_{IF}$), 22GHz ($2f_{LO}$), 14GHz ($f_{IF}+f_{LO}$), 8GHz ($f_{LO}-f_{IF}$), 19 ($2f_{LO}-f_{IF}$), etc. The input signal feedthrough is about -120dBm, the output at 14GHz is about -60dBm, since the input power is -41dBm, the conversion loss is approximately 19dB.

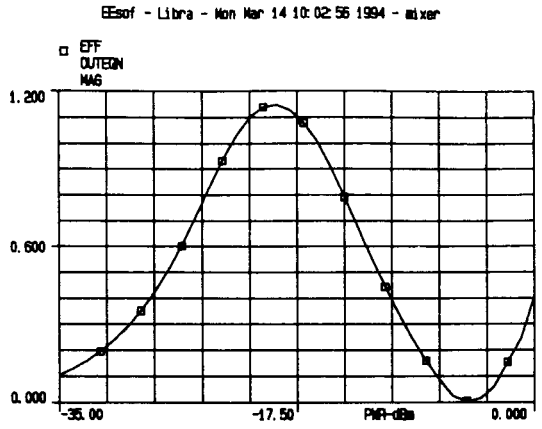

Fig. 4.24 Simulation power efficiency of RTD mixer vs. LO input power

Compared to the theoretical result shown in Fig. 3.11, the plot above shows that the power efficiency of the RTD mixer increases until the optimum LO drive level is reached, and then decreases as the mixer compresses at high LO drive levels. The maximum efficiency is about 1.2%, which is approximately equal to 19dB of conversion loss.

The layout of the RTD mixer is shown below:

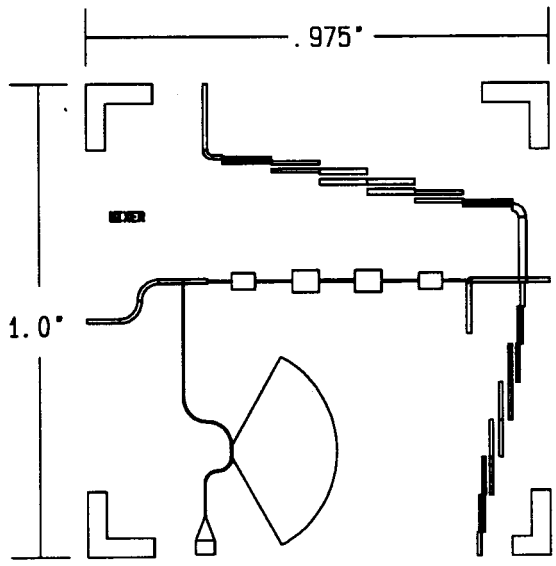

Fig. 4.25 ACADEMY layout of the RTD mixer

4.2 RTD Multiplier

The simple sketch of the RTD multiplier is shown in Fig. 4.26. A, and B are matching transmission lines between the RTD and the two filters. Instead of a bandpass filter, a lowpass filter is chosen to be the IF port frequency selective network for the same reasons as was mentioned before in the mixer section. The IF input frequency is 7GHz and the RF output frequency is 14GHz.

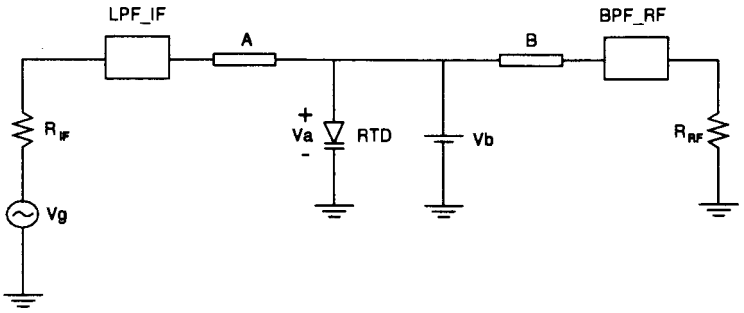

Fig. 4.26 Simple sketch of the RTD multiplier

4.2.1 Principles of IF LPF Design for the RTD Multiplier

Considering the frequency existing in each port, the IF LPF for the multiplier should be able to let the signals with frequencies around 7GHz or less pass through, and filter out the signals with frequencies around 14GHz or higher. Thus the pass-band edge frequency f1 is chosen to be 8GHz, and the stop-band frequency f' is chosen to be 14 GHz.

Let Lar=0.01dB, $\omega 1 = 2\pi f1 = 16\pi(Grad/s)$, L'ar=55dB and $\omega' = 2\pi f' = 28\pi(Grad/s)$, using Eqn. (4-1), one can get the minimum number of reactive elements n=8.6826. To get a symmetrical structure, n needs to be odd, so n=9 is chosen for the LPF.

Through the same procedure as described in section 4.1.1, chosing Z_h=77ohm and Z_l=27ohm, the electrical length of each transmission line can be obtained. The in-band and wide band attenuation plots are shown below:

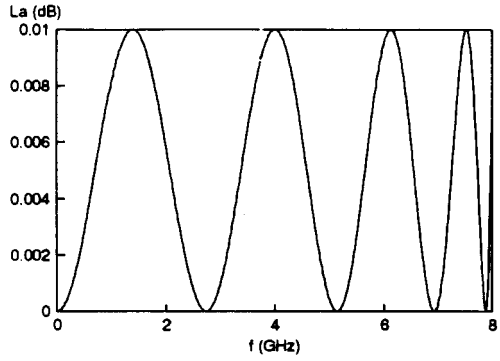

Fig. 4.27 Theoretical result of inband LPF of the multiplier

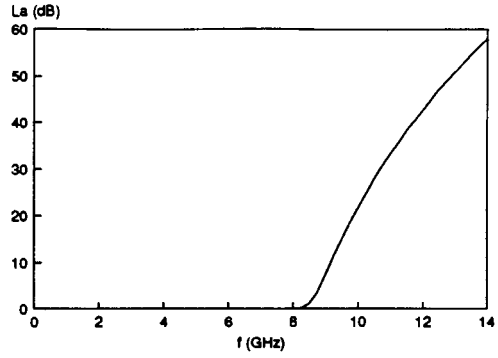

Fig. 4.28 Theoretical result of wide band LPF of the multiplier

The RF BPF of the RTD multiplier is the same as the RF BPF of the RTD mixer.

4.2.2 Simulation of the Circuit Components of the RTD Multiplier

Through the same procedure as the one described in section 4.1.4, the optimized or simulation results of the circuit components can be obtained:

A) LPF of the RTD multiplier

The ACADEMY schematic of the LPF of the RTD multiplier is similar to that of the LPF of the RTD mixer. The simulation results are shown below:

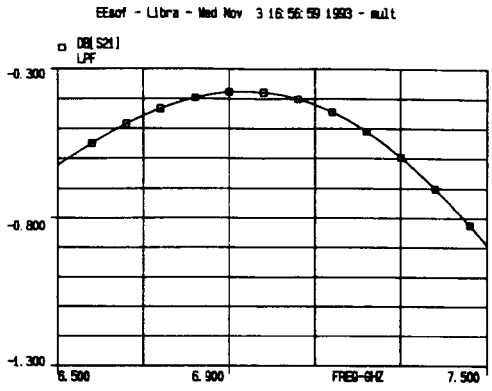

Fig. 4.29 Simulation result of the inband LPF of the RTD multiplier

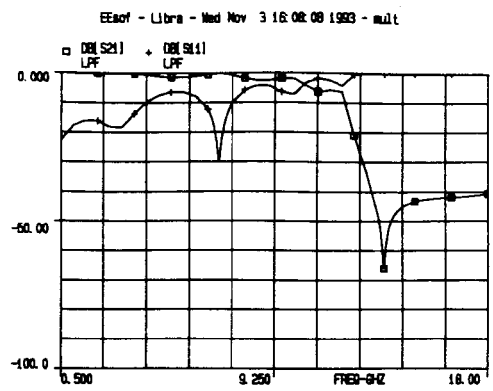

Fig. 4.30 Simulation result of the wide band LPF of the RTD multiplier

B) RTD I-V curve of the RTD multiplier

The ACADEMY schematic model of RTD and the simulation RTD I-V curve of the RTD multiplier are the same as those of the RTD mixer.

C) Bias block of the RTD multiplier

The ACADEMY schematic of the RTD multiplier bias block is shown in Fig. 4.31, the optimized simulation result of the RTD multiplier bias block is shown in Fig. 4.32.

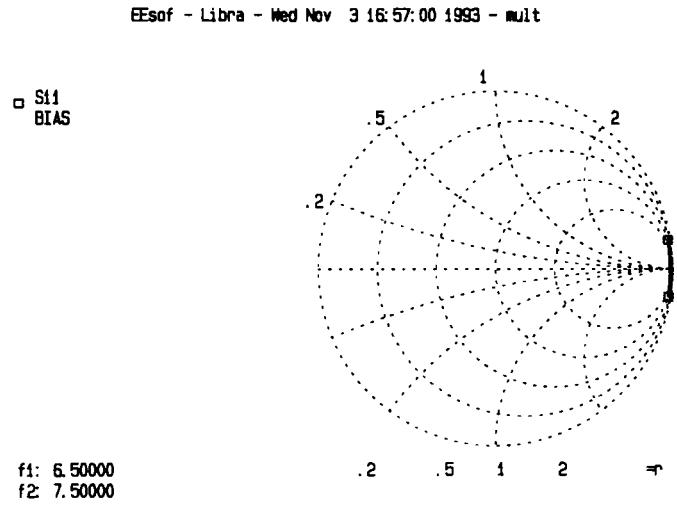

Fig. 4.32 Simulated S11 of the RTD multiplier bias block

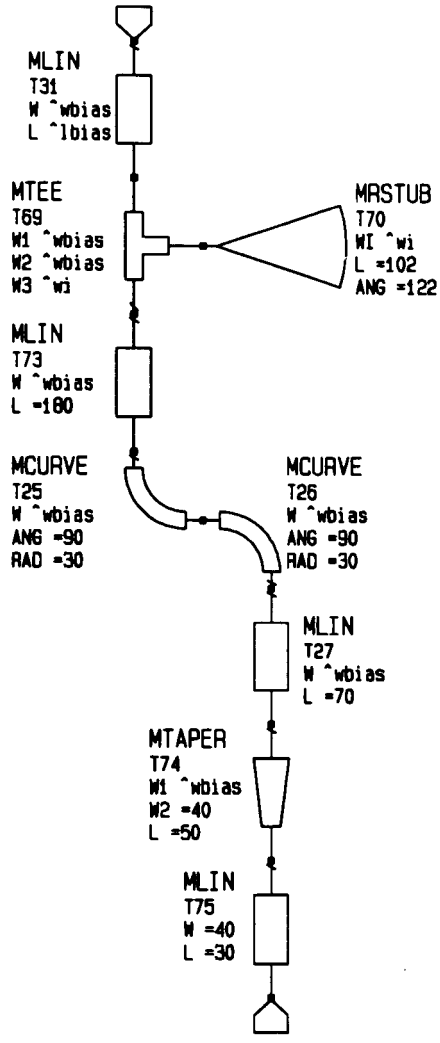

Fig. 4.31 ACADEMY schematic of the bias block of the RTD multiplier

4.2.3 Simulation of the RTD Multiplier

The individual components can be cascaded together to realize the RTD multiplier.

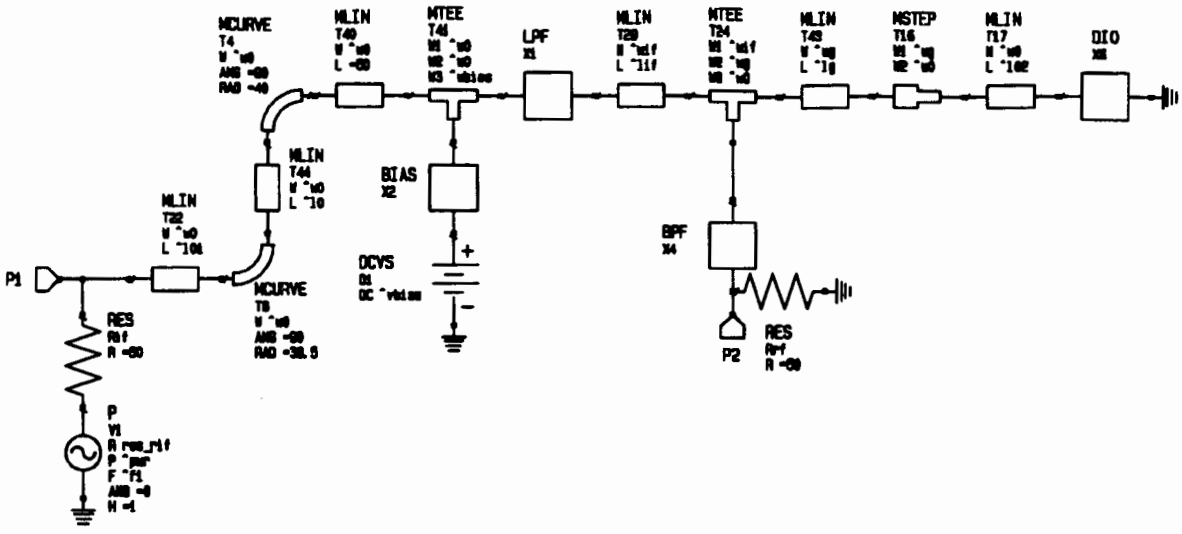

Fig. 4.33 ACADEMY schematic of the RTD multiplier

Considering the size limitation of the circuit, the final maximum power efficiency of the RTD multiplier was optimized to 0.95%, which is not the best performance that can be obtained. The final simulation results of the RTD multiplier are shown below:

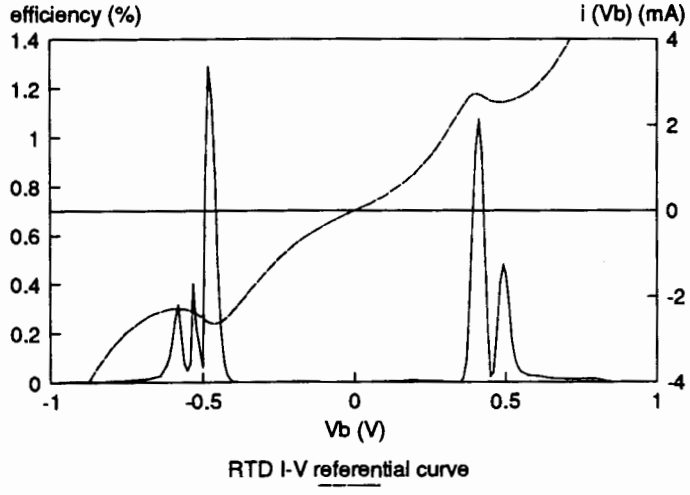

Fig. 4.34 Simulation power efficiency of RTD multiplier vs. DC bias voltage.

Compared to the theoretical result shown in Fig. 3.14, the plot above shows that two peaks in the power efficiency of the RTD multiplier occur at the peak and valley voltages (V_P, V_V), with the one occurring at V_P much higher than the other. However, the negative part is not symmetrical to the positive part due to the asymmetry of the RTD I-V curve in simulation.

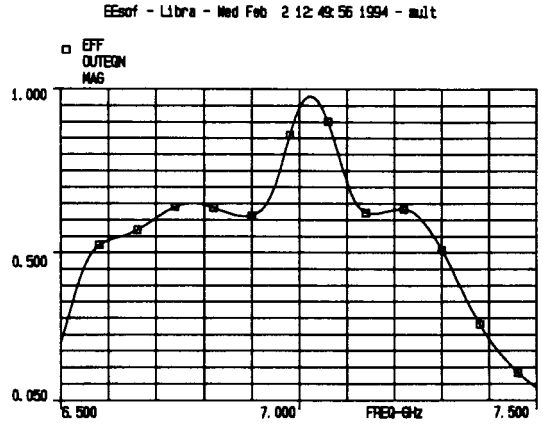

Fig. 4.35 Simulation power efficiency of RTD multiplier vs. inband frequency

The plot above shows that within the inband frequency, the RTD mixer obtained a maximum efficiency of 0.95% at the input frequency of 7.02GHz.

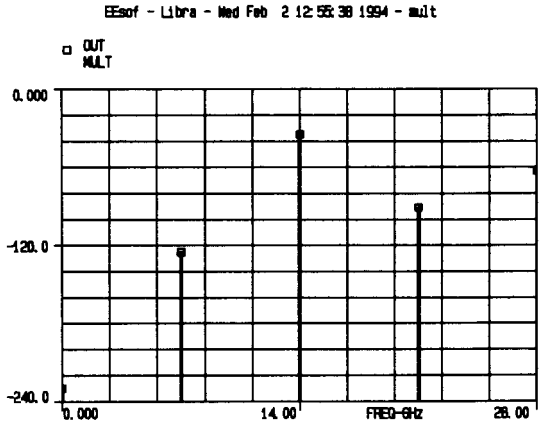

Fig. 4.36 Simulation power spectrum density of RTD multiplier vs. wide band frequency

When a sinusoidal frequency (f1) is applied to a multiplier, the output signal of the multiplier will contain the frequency components at its harmonics (f1, 2f1, 3f1, etc) and DC. Fig. 4.36 shows that, the multiplier converts the input signal at f1=7GHz into the signals having frequency components at DC, 7GHz (f1), 14GHz (2f1), 21GHz (3f2), 28GHz (4f1), etc. The input signal feedthrough is more than -120dBm, the output at 14GHz is about -34dBm, since the input power is -14.4 dBm, the conversion loss is approximately -20dB.

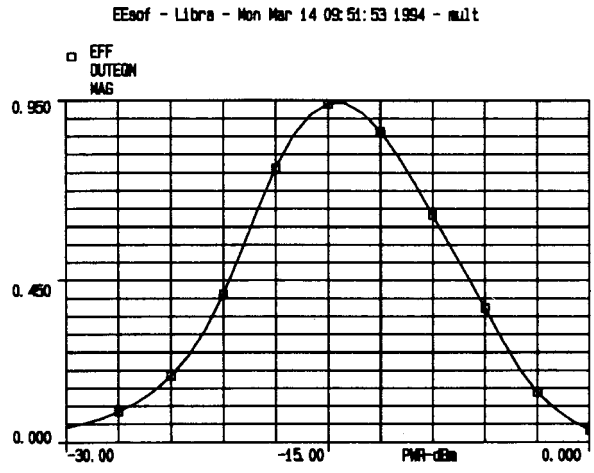

Fig. 4.37 Simulation power efficiency of RTD multiplier vs. input power

Compared to the theoretical result shown in Fig. 3.19, the plot above shows that the power efficiency of the RTD multiplier increases until the optimum P_{IN} level is reached, and then decreases as the multiplier compresses at high P_{IN} levels. The maximum power efficiency is about 0.95%, which is about -20dB of conversion loss.

The layout of the RTD multiplier is shown below:

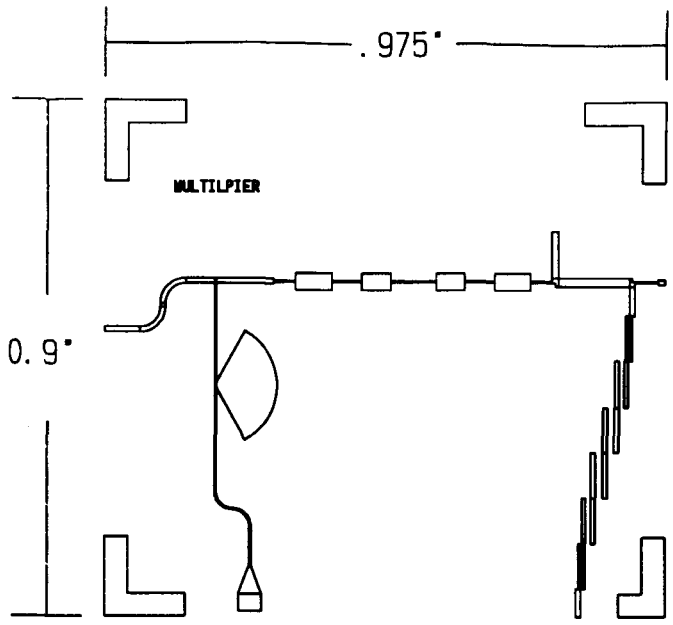

Fig. 4.38 ACADEMY layout of the RTD multiplier

4.3 Fabrication of the RTD Mixer and Multiplier

After the design, the RTD mixer and multiplier circuits and their circuit components (filters, bias, etc) were laid out in one template by ACADEMY. Through a package MICmask, the drawing of the template was transferred to Gerber and mask files which were sent out for fabrication. The whole template consisting of four circuit units is shown below:

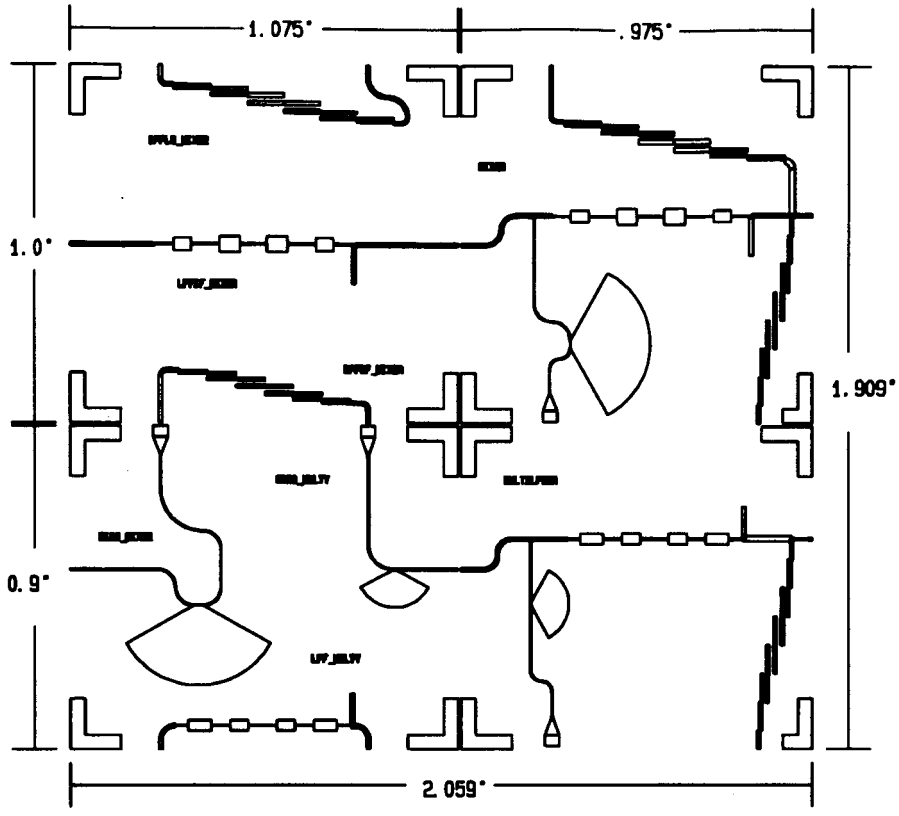

Fig. 4.39 ACADEMY layout of the whole template consisting of RTD mixer and multiplier, and their circuit components.

5 MEASUREMENT OF RTD MIXER AND MULTIPLIER

After the circuits were fabricated, one can test the passive parts of the RTD mixer and multiplier (filters, bias blocks) independently.

Diced from an RTD wafer and stuck on one board with wax, the RTD chips were probed on a cascade probing station. The DC I-V curves of the RTDs were measured with an HP4145B semiconductor parameter analyzer. Two RTDs whose I-V characteristics are similar to that of the RTD used in the simulation (section 4.1.5) were picked. After the cleaning procedure in the clean room, the two RTDs were mounted to the housing and wirebonded to the RTD mixer and multiplier circuits, respectively.

5.1 RTD Mixer

5.1.1 Circuit Components of the RTD Mixer

The following circuit components of the mixer were terminated with 50Ω connectors and were measured with an HP8510A network analyzer, shown in Fig. 5.1. Calibration of the test set was needed before each measurement. Since the components are symmetrical structures, their S parameters are symmetrical too, so only S21 and S11 are shown.

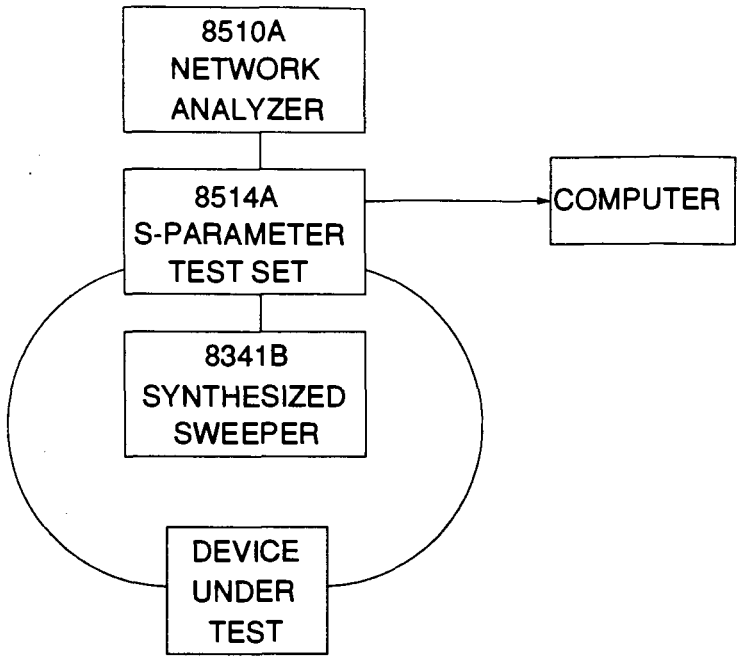

Fig. 5.1 Test devices for measuring the passive parts of the RTD mixer and multiplier

A) Measured results of the IF LPF of the RTD mixer

The measured results of the IF LPF of the RTD mixer are plotted below:

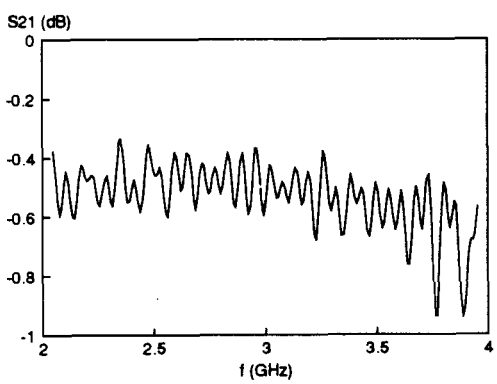

Fig. 5.2 Measured result of inband LPF of the RTD mixer

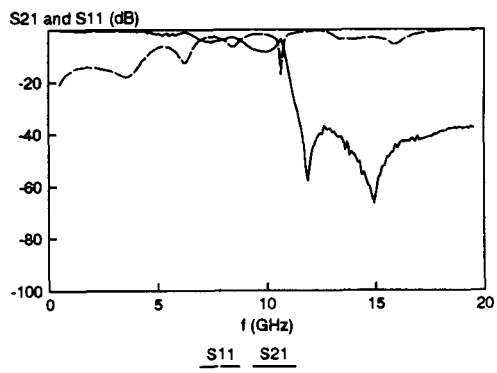

Fig. 5.3 Measured results of wide band LPF of the RTD mixer

Compared to the simulation result shown in Fig. 4.9, whose inband transmission attenuation S21 of the IF LPF of the mixer is about -0.3dB, with a ripple of 0.2dB, the measured result

shown in Fig. 5.2 has a transmission attenuation of -0.5dB, with a ripple of 0.3dB. Comparing the wide band attenuation results shown in Fig. 4.10 and Fig. 5.3, both results have a small attenuation and return loss at 3GHz, significant attenuation and return loss at 11 and 14GHz.

B) Measured results of the RF BPF of the RTD mixer

The measured results of the RF BPF of the RTD mixer are plotted below:

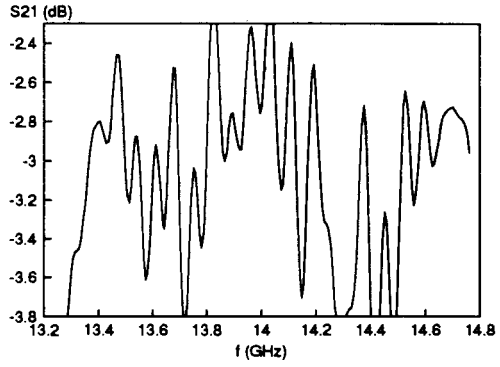

Fig. 5.4 Measured result of inband RF BPF of the RTD mixer

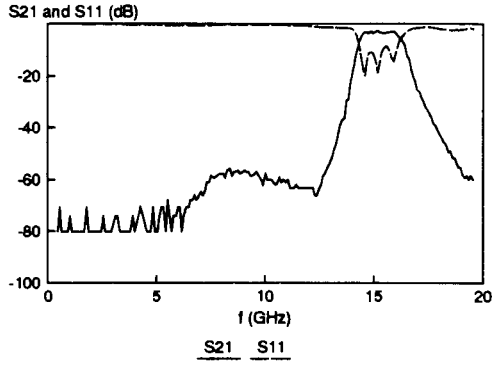

Fig. 5.5 Measured results of wide band RF BPF of the RTD mixer

Compared to the simulation result shown in Fig. 4.12, whose inband transmission attenuation S21 of the RF BPF of the mixer is about -2.3dB, with a ripple of more than 1dB, the measured result shown in Fig. 5.4 has a transmission attenuation of -3dB, with a ripple of 1.5dB. Comparing the wide band attenuation results shown in Fig. 4.13 and Fig. 5.5, both results have a small attenuation and return loss at 14GHz, significant attenuation and return loss at 3 and 11GHz.

C) Measured results of the LO BPF of the RTD mixer

The measured results of the LO BPF of the RTD mixer are plotted below:

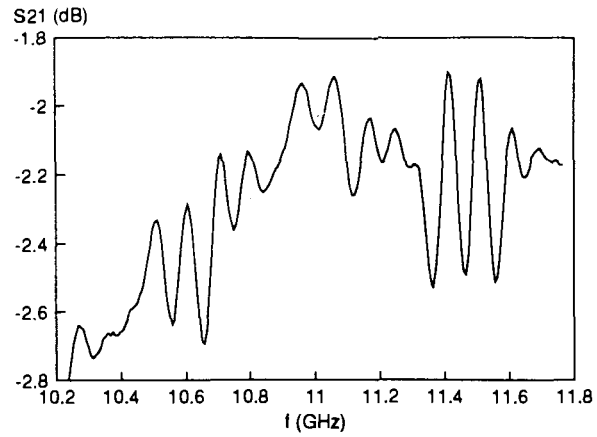

Fig. 5.6 Measured result of inband LO BPF of the mixer

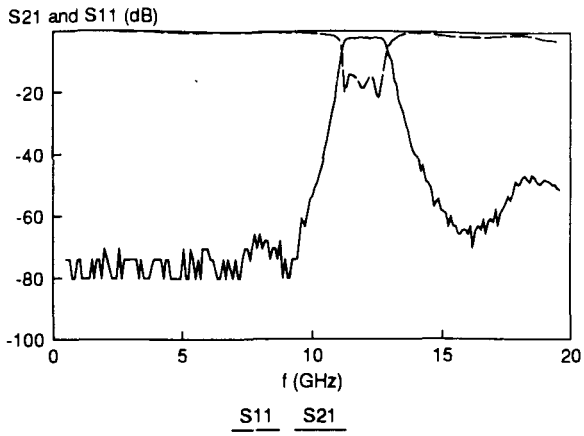

Fig. 5.7 Measured results of wide band LO BPF of the mixer

Compared to the simulation result shown in Fig. 4.14, whose inband transmission attenuation S21 of the RF BPF of the mixer is about -1.95dB, with a ripple of more than 0.3dB, the measured result shown in Fig. 5.6 has a transmission attenuation of -2.35dB, with a ripple of 0.7dB. Comparing the wide band attenuation results shown in Fig. 4.15 and Fig. 5.7, both results have a small attenuation and return loss at 11GHz, significant attenuation and return loss at 3 and 14GHz.

D) Measured results of the bias block of the RTD mixer

The RTD mixer bias block is a one port network, so only S11 was measured and shown in the smith chart:

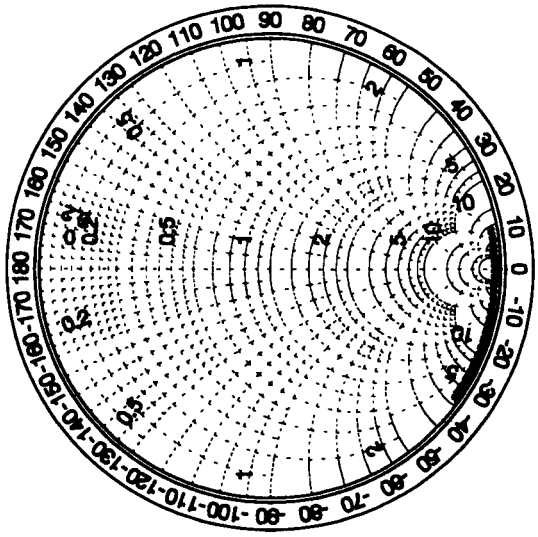

Fig. 5.8 Measured S11 of the bias block of the RTD mixer (f=2.5 to 3.5GHz)

Comparing the results shown in Fig. 4.19 and Fig. 5.8, both have a very high impedance at frequencies around 3GHz. The measured result in Fig. 5.8 is not centered to the real impedance line as was in the simulation result, due to the phase delay of the bias block.

E) Measured results of the RTD I-V Curve of the RTD mixer

The measured RTD I-V curve of the mixer is shown below:

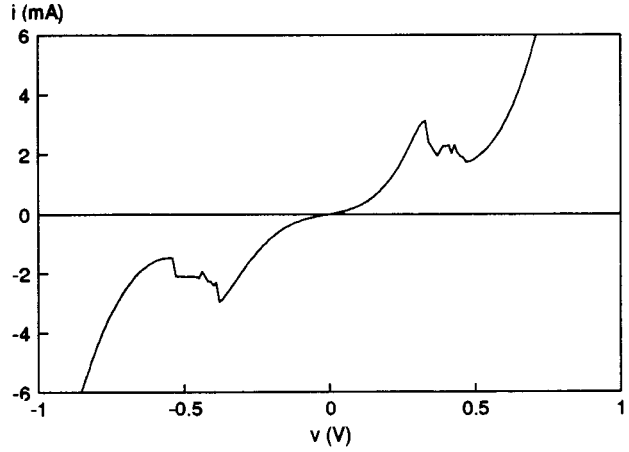

Fig. 5.9 Measured RTD I-V curve of the RTD mixer

The measured result shown in Fig. 5.9 is very similar to the simulation result shown in Fig. 4.17. For the simulation I-V curve, V_P=0.4V, V_V=0.48V, I_P=2.72mA, and I_V=2.52mA; for the measured I-V curve, V_P=0.32V, V_V=0.47V, I_P=3.12mA, and I_V=1.72mA.

5.1.2 Measurement of the RTD Mixer

A) Power efficiency (or conversion Loss) of the RTD mixer

The power efficiency of the RTD mixer was measured with an HP8341B synthesized sweeper at the IF input port and another at the LO input port. The HP2782 spectrum analyzer was connected at the RF output port, and DC power supply and DC voltage meter at the bias port, as shown below:

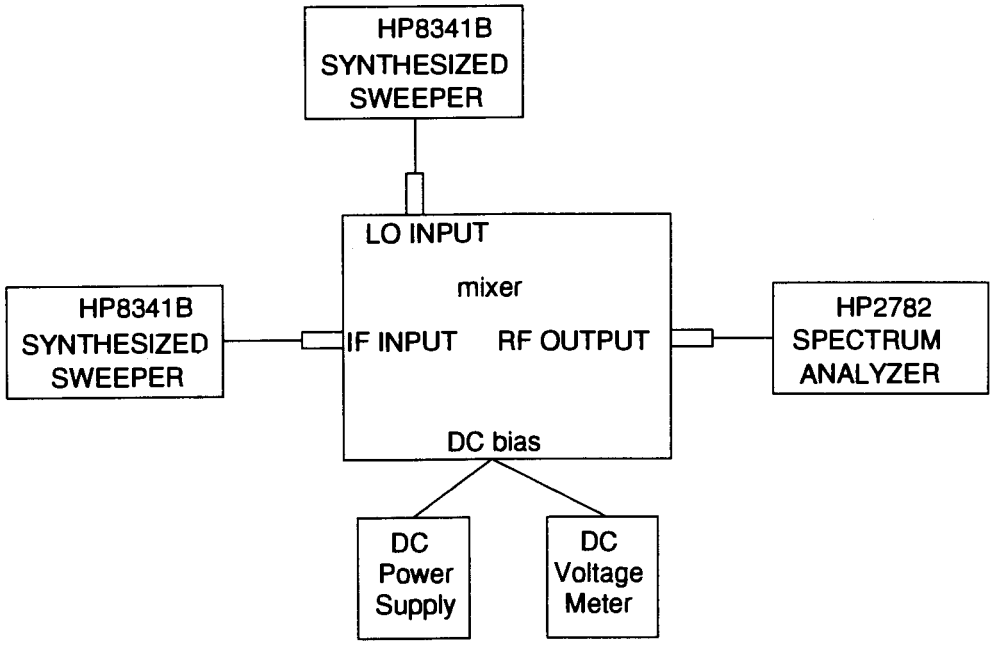

Fig. 5.10 Devices for measuring the power efficiency of the RTD mixer

1) Power efficiency of the RTD mixer versus the LO power P_{LO}

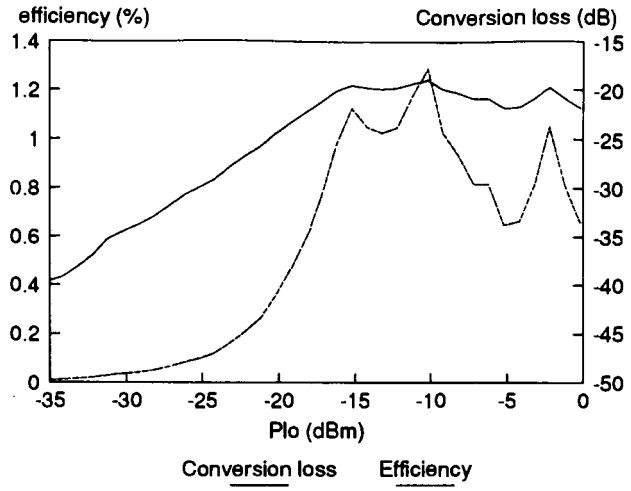

Fig. 5.11 Measured power efficiency and conversion loss of the RTD mixer versus P_{LO}

Compared to the simulation result shown in Fig. 4.24, the plot above shows that the power efficiency of the RTD mixer increases until the optimum LO drive level is reached, and then decreases as the mixer compresses at high LO drive levels. The maximum power efficiency is about 1.2%.

2) Power efficiency of the RTD mixer versus Vb

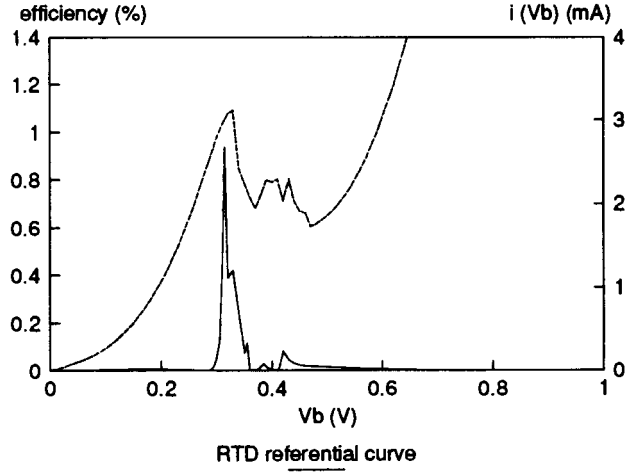

Fig. 5.12 Measured power efficiency of the RTD mixer versus Vb.

Compared to the theoretical and simulation results shown in Fig. 3.6 and Fig. 4.21, respectively, the plot above shows that two peaks in the power efficiency of the RTD

mixer occur at the peak and valley voltages (V_P, V_V), with the one occurring at V_P much higher than the other. However, in the NDR region, the efficiency of the RTD mixer measured with the increasing bias voltage sweep is quite different from that measured with the decreasing bias voltage sweep. This phenomenon is called hysteresis. Also around this area, the efficiency is very sensitive to the bias voltage. These show the instability of the RTD in the NDR region.

3) Power efficiency of the mixer versus inband frequency

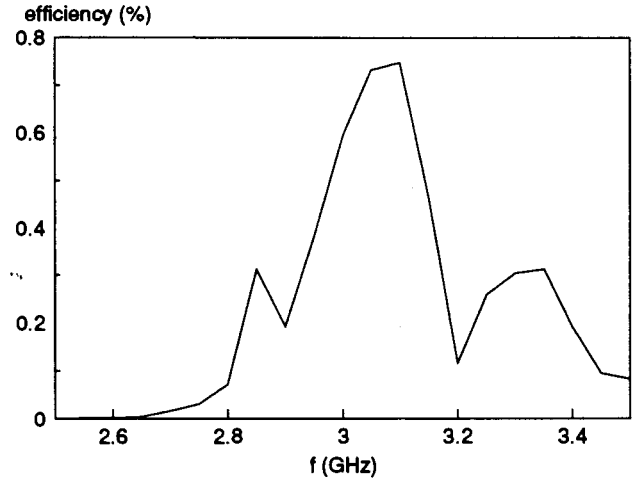

Fig. 5.13 Measured power efficiency of the RTD mixer versus inband frequency.

The plot above shows that within the inband frequency, the RTD mixer obtained a maximum efficiency of 0.75% at the input frequency of 3.1GHz.

B) 1-dB compression point

1-dB compression point is a measure of the maximum IF input signal level for which the mixer will provide linear operation. The conversion loss remains constant over a specified input signal range. When the input signal level exceeds a certain amount, usually when the

IF signal level is within 10 dB of the LO drive level, the constant ratio between RF and IF will begin to change. The point at which the constant ratio has changed by 1 dB is described as the 1-dB compression point.

The conversion compression of the mixer is measured with the same devices shown in Fig. 5.10. In Fig. 5.14, the 1-dB compression point is -30dB.

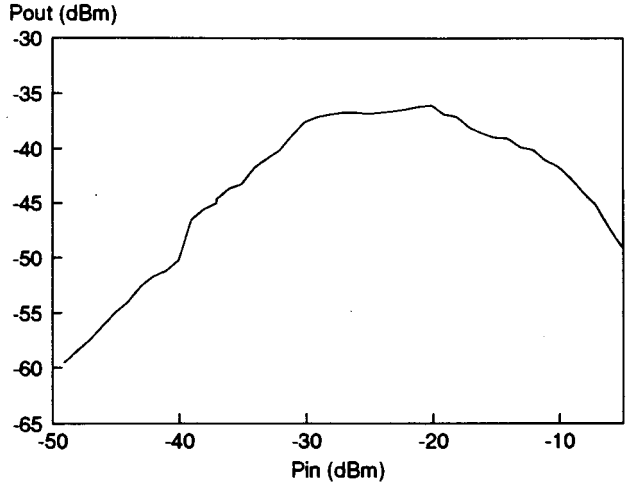

Fig. 5.14 Measured IF to RF conversion compression of the RTD mixer

C) Two-tone, third order intermodulation distortion

When two sinusoidal frequencies (f1 and f2) are applied to a mixer, the output signal of the mixer will contain frequency components at DC, f1, f2, 2f1, 2f2, 3f1, 3f2, $f1 \pm f2$, $2f1 \pm f2$, and $2f2 \pm f1$, ..., due to the nonlinearity of the mixer. The frequencies $2f1 \pm f2$ and $2f2 \pm f1$ are third-order intermodulation products. Usually, the third-order intermodulation products at 2f1-f2 and 2f2-f1 are very close to the fundamental frequencies f1 and f2, and fall within the output bandwidth of the mixer, producing distortion in the output. The third-order intercept point is defined as the point where the power at f1 and the power at 2f1-f2 intercept.

The third-order intermodulation product output power at 2f1-f2 versus the input power at f1 is show in Fig. 5.16. The setup for measuring the third order intermodulation distortion of the RTD mixer is shown below:

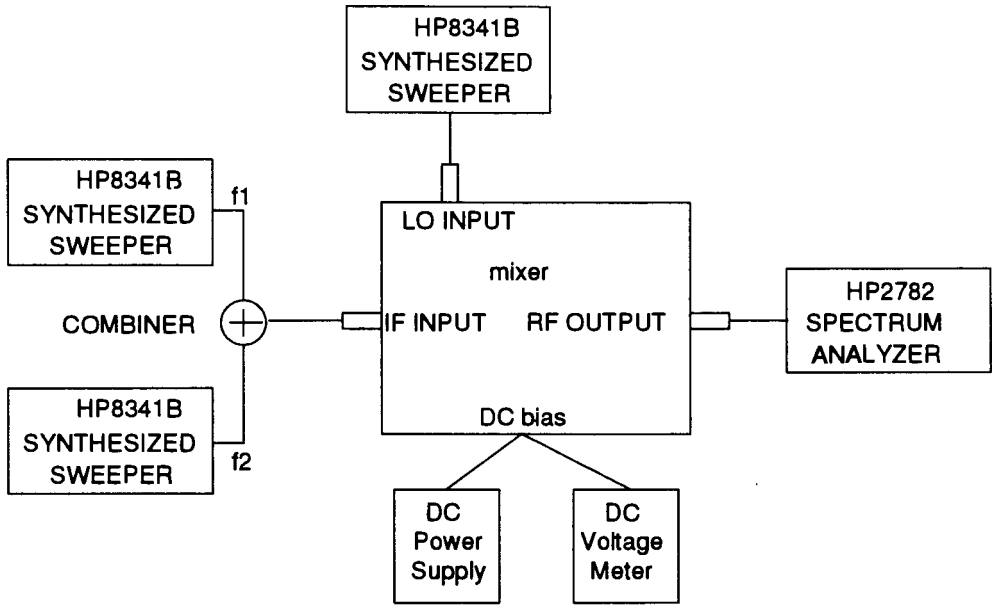

Fig. 5.15 Setup for measuring the third order intermodulation distortion of the RTD mixer.

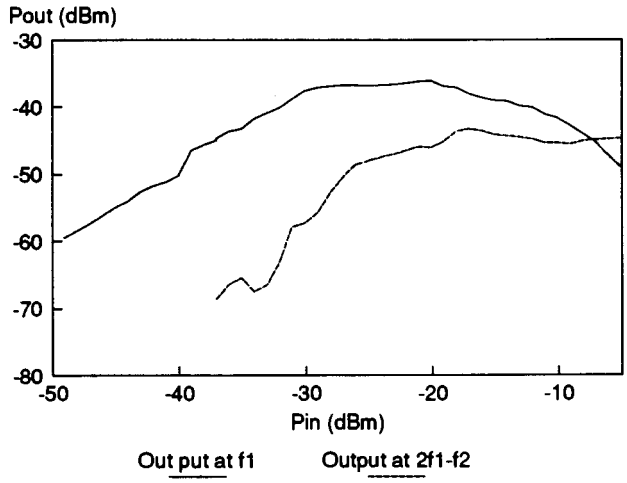

Fig. 5.16 Measured third order intermodulation distortion of the RTD mixer

The plot above shows that, the slope of power at f1 is approximately 1 and that of power at 2f1-f2 is approximately 3. This occurs because the power of the third-order intermodulation product is proportional to the cube of the input signal amplitude. The third-order intercept point occurs at about -10dB.

5.2 RTD Multiplier

5.2.1 Circuit Components of the RTD Multiplier

Through the same procedure as the one described in section 5.1.1, the following measured results of the passive parts of the RTD multiplier are obtained:

A) Measured Results of the LPF of the RTD Multiplier

The measured results of the LPF of the RTD multiplier are shown below:

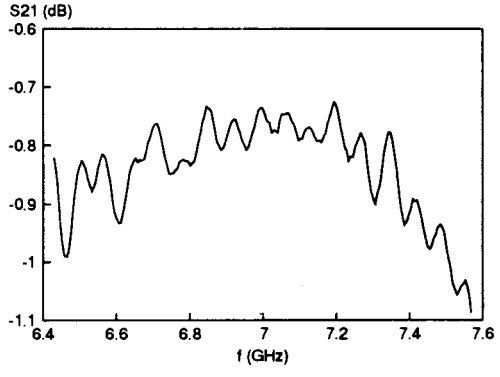

Fig. 5.17 Measured result of inband LPF of the RTD multiplier.

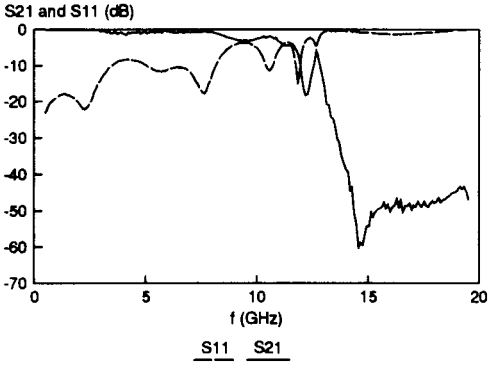

Fig. 5.18 Measured results of wide band LPF of the RTD multiplier.

Compared to the simulation result shown in Fig. 4.30, whose inband transmission attenuation S21 of the LPF of the multiplier is about -0.6dB, with a ripple of 0.4dB, the measured result shown in Fig. 5.17 has a transmission attenuation of -0.9dB, with a ripple of 0.35dB.

Comparing the wide band attenuation results shown in Fig. 4.29 and Fig. 5.18, both results have a small attenuation and return loss at 7GHz, significant attenuation and return loss 14GHz.

B) Measured results of the RF BPF of the RTD multiplier

The RF BPF of the RTD multiplier is the same as the RF BPF of the RTD mixer.

C) Measured results of the RTD I-V curve of the multiplier

The measured RTD I-V curve of the multiplier is shown below:

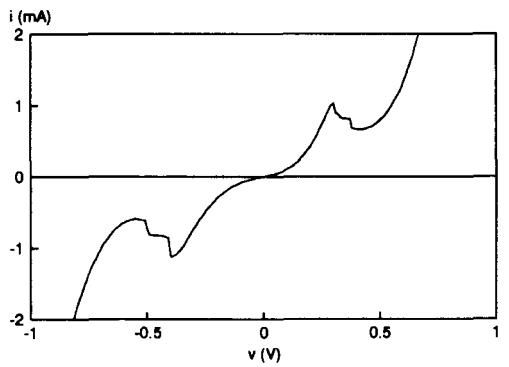

Fig. 5.19 Measured RTD I-V curve of the multiplier

The measured result shown in Fig. 5.19 is very similar to the simulation result shown in Fig. 4.17. For the simulation I-V curve, V_P=0.4V, V_V=0.48V, I_P=2.72mA, and I_V=2.52mA; for the measured I-V curve, V_P=0.3V, V_V=0.41V, I_P=1.03mA, and I_V=0.66mA.

D) Measured results of the bias block of the RTD multiplier

The bias block of the RTD multiplier is a one port network, so only S11 was measured and shown in the smith chart:

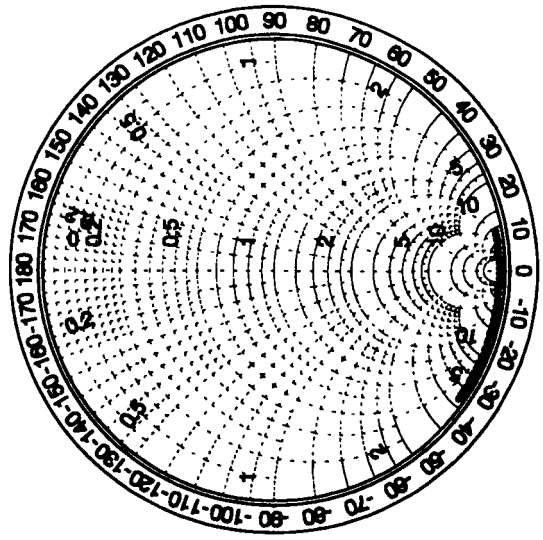

Fig. 5.20 Measured S11 of the RTD multiplier bias block (f=6.5 to 7.5GHz)

Comparing the results shown in Fig. 4.19 and Fig. 5.8, both have a very high impedance at frequencies around 7GHz. The measured result in Fig. 5.20 is not centered to the real impedance line as was in the simulation result, due to the phase delay of the bias block.

5.2.2 Power Efficiency of the RTD Multiplier

The power efficiency of the RTD multiplier was measured with an HP8341B synthesized sweeper at the IF input port of the multiplier, an HP2782 spectrum analyzer at the RF output port of the multiplier, a DC power supply and a voltage meter at the bias port.

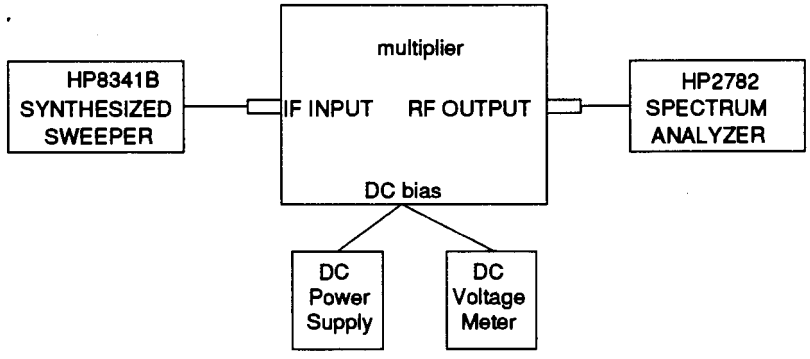

Fig. 5.21 Devices for Measuring the power efficiency of the RTD multiplier.

The measured power efficiencies of the RTD multiplier are shown below:

A) Power efficiency of the RTD multiplier versus the input power P_{IN}

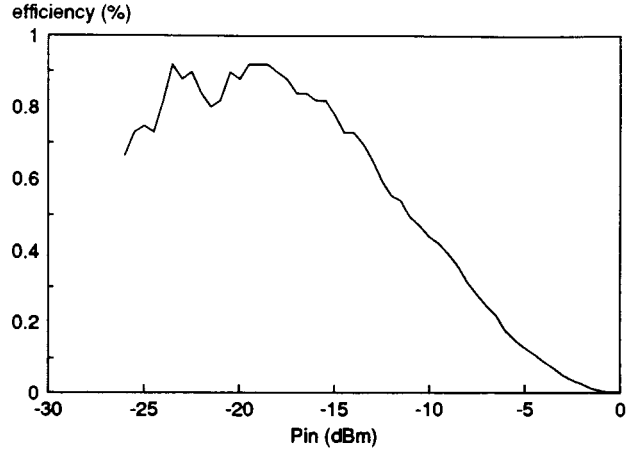

Fig. 5.22 Measured power efficiency of the RTD multiplier versus the input power P_{IN}.

Compared to the simulation result shown in Fig. 4.37, the plot above shows that the power efficiency of the RTD multiplier increases until the optimum P_{IN} level is reached, and then decreases as the multiplier compresses at high P_{IN} levels. The maximum power efficiency is about 0.95%.

B) Power efficiency of the RTD multiplier versus Vb

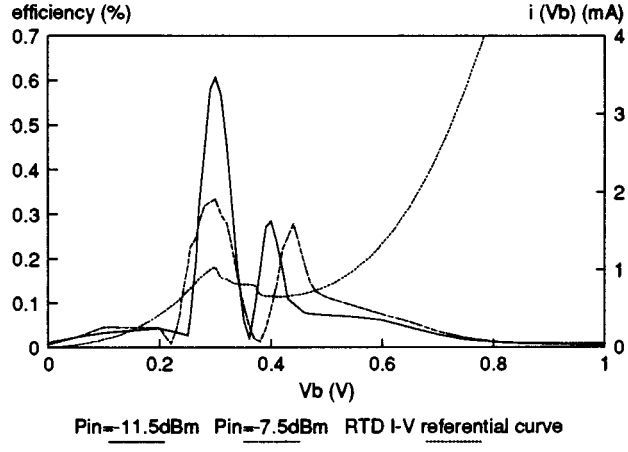

Fig. 5.23 Measured power efficiency of the RTD multiplier versus Vb.

Compared to the simulation result shown in Fig. 4.34, the plot above shows that two peaks in the power efficiency of the RTD multiplier occur at the peak and valley voltages (V_P, V_V), with the one occurring at V_P much higher than the other.

C) Power efficiency of the multiplier versus inband frequency

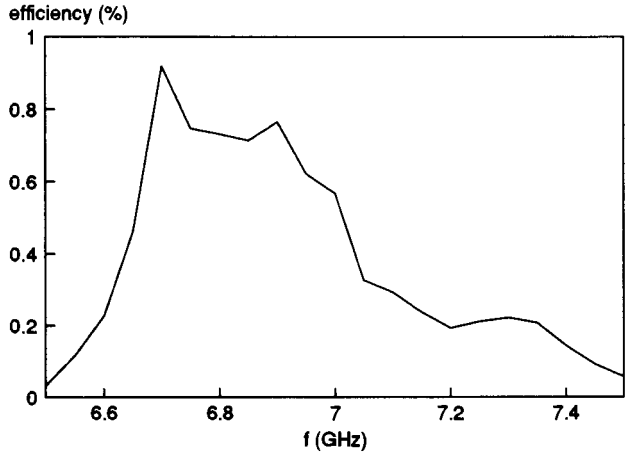

Fig. 5.24 Measured power efficiency of the RTD multiplier versus inband frequency.

The plot above shows that within the inband frequency, the RTD multiplier obtained a maximum efficiency of 0.95% at the input frequency of 6.7GHz.

6 CONCLUSIONS

In this thesis, the characteristics of RTDs and their circuits were studied through theoretical analysis, ACADEMY simulation and measurement. Through these studies, several conclusions are drawn:

1) Good accuracy of the RTD modeling and the simulation on ACADEMY

   Comparing the simulated results shown in chapter 4 and the measured results shown in chapter 5, one can tell that the modeling procedure provided very accurate simulation results. For example, the maximum power efficiency of the RTD multiplier is designed to be 0.95% in the simulation (Fig. 4.37), in the measurement 0.91% was obtained, which includes the consideration of the transmission losses of the connecting cables at the IF port (7GHz) and the RF port (14GHz), the transmission losses of the IF LPF, the RF BPF and the 50ohm connectors. Also if the re-simulation of the RTD is processed, the two results will be in much better agreement.

2) The theoretical results show that at microwave frequencies, the RTD's parallel capacitor can be neglected compared to its parallel resister, thus only the I-V curve of the RTD is applied in the theoretical analysis. Also, Comparing the theoretical results shown in chapter 3 with the measured results shown in chapter 5, one can tell that the theoretical results have a much higher efficiency than the measured results. This is because only the ideal situation (such as perfect matching, no insertion loss of the filters, etc) is considered in the theoretical analysis. In reality, the perfect matching requires much longer matching microstrip transmission lines, which is difficult to realize due to the limitation of the circuit size. However the analysis does provide a quantitative relationship between the output and input parameters, and makes the prediction of the performance of RTD circuits much easier.

3) An RTD is useful in microwave mixer and multiplier applications.

In comparison to the Schottky barrier diode and varactor diode, an RTD has a stronger nonlinearity which allows more efficient harmonic generation with smaller input signal levels, and more efficient higher-order harmonic generation with unoptimized idler terminations. The maximum harmonic generation efficiency of an RTD device is significantly higher than the $1/n^2$ (n is the harmonic number) value that applies to standard resistive multipliers because of its negative resistance. Thus a much lower input power is required to drive the RTD multiplier, and much lower LO and IF power is necessary to drive the RTD mixer. This means that expensive, high power microwave amplifiers are no longer necessary to amplify input signals of the RTD circuits to the required levels.

4) Short comings of the RTD circuits

First, the RTD mixer and multiplier are very sensitive to the DC bias voltage. During the measurement, it was found that sometimes even 0.002V difference in the DC bias voltage could cause a very significant difference in the power efficiency. A DC power supply with very fine resolution (0.001V) was required in the measurement of the two RTD circuits.

Second, the RTD circuits have potential instability problems. For some of the RTDs, when the DC bias voltage was near to or in the NDR region, the RTD circuits oscillated. Also, in the NDR region, the efficiency of the RTD circuits measured with the increasing bias voltage sweep is quite different from that measured with the decreasing bias voltage sweep. This is called hysteresis.

Third, the RTD circuits has noise floor problem. Since the RTD operates at very low signal levels in order to get high efficiency, the noise floor of the circuits becomes a more significant factor.

7 REFERENCES

[1] L. Esaki and R. Tsu, "Superlattice and negative differential conductivity in semiconductors," *IBM J. res. develop.*, Vol. 24, 1970. pp. 61-65.

[2] R. Tsu and L. Esaki, *Appl. phys. Lett.*, Vol. 22, 1973, pp. 562.

[3] L.L. Chang, L. Esaki and R. Tsu, *Appl. phys. Lett.*, Vol. 24, 1974. pp. 593.

[4] T.C.L.G. Sollner, W.D. Goodhue, P.E. Tannenwald, C.D. Parker, and D.D. Peck, "Resonant tunneling through quantum wells at frequencies up to 2.5 THZ," *Appl. phys. Lett.*, Vol. 43, Sept. 1983, pp. 588-590.

[5] T.C.L.G. Sollner, P.E. Tannenwald, D.D. Peck, and W.D. Goodhue, "Quantum well oscillators" *Appl. phys. Lett.*, Vol. 45, No. 12, 15 December 1984.

[6] W.D. Goodhue, T.C.L.G. Sollner, H.Q. Le, E.R. Brown, and B.A. Vojak, "Large room temperature effects form resonant tunneling through AlAs barriers," *Appl. phys. Lett.*, Vol. 49, 1986, pp. 1086.

[7] E.R. Brown, T.C.L.G. Sollner, W.D. Goodhue, and C.D. Parker, "Millimeter-band oscillations based on resonant tunneling in a double-barrier diode at room temperature" *Appl. phys. Lett.*, Vol. 50, No. 2, 12 January 1987.

[8] T.C.L.G. Sollner, E.R. Brown, W.D. Goodhue, and H.Q. Le, "Observation of millimeter-wave oscillations form resonant tunneling diodes and some theoretical considerations of ultimate frequency limits," *Appl. phys. Lett.*, Vol. 50, No. 6, 9 February 1987.

[9] E.R. Brown, T.C.L.G. Sollner, C.D. Parker, W.D. Goodhue, and C.L. Chen, "Oscillations up to 420 GHz in GaAs/AlAs resonant tunneling diodes," *Appl. phys. Lett.*, Vol. 55, No. 17, 23 October 1989, pp. 1777-1779.

[10] N.C. Kluksdahl, A.M. Krimfan, and D.K. Ferry, "Role of structure sizes in determining the characteristics of the resonant tunneling diode," *Solid-state electronics*, Vol. 32, No. 12, 1989, pp. 1273-1276.

[11] E.R. Brown, C.D. Parker, A.R. Calawa, M.J. Manfra, C.L. Chen, L.J. Mahoney, and W.D. Goodhue, "High frequency resonant-tunneling oscillators," *Microwave and optical technology letters*, Vol. 4, No. 1, January 5 1991.

[12] E.R. Brown, C.D. Parker, K.M. Molvar, and M.K. Connors, "Recent advances in resonant-tunneling-diode oscillators," *IEEE proceedings, second international symposium on space terahertz technology*, Feb. 26-28, 1991, pp. 133-144.

[13] M.W. Dellow, P.H. Beton, C.J.G.M. Langerak, T.J. Foster, P.C. Main, L. Eaves, M. Henini, S.P. Beaumont, and C.D.W. Wilkinson, "Resonant tunneling through the bound states of a single donor atom in a quantum well," *Physical review letters*, Vol. 68, No. 11, 16 March 1992.

[14] P.H. Beton, M.W. Dellow, P.C. Main, T.J. Foster, L. Eaves, A.F. Jezierski, and M. Henini, "Edge effects in a gated submicron resonant tunneling diode," *Appl. phys. Lett.*, Vol. 60, No. 20, 18 May 1992.

[15] E.R. Brown, C.D. Parker, and T.C.L.G. Sollner, "Effect of quasibound-state lifetime on the oscillation power of resonant tunneling diodes," *Appl. phys. Lett.*, Vol. 54, No. 10, 6 March 1989.

[16] V. P. Kesan, A. Mortazawi, D. P, Neikirk, and T. Itoh, "Microwave and millimeter-wave QWITT diode oscillator," *IEEE MTT-S int. microwave symp. digest,* June 1989, pp. 487-490.

[17] Karl D. Stephan and Sai-Chu Wong, "Lossy-line stabilization of negative-resistance diodes for integrated-circuit oscillators," *IEEE Proceedings, second international symposium on space terahertz technology,* Feb. 26-28, 1991, pp. 154-162.

[18] A. Mortazawi, V. P. Kesan, D. P, Neikirk, and T. Itoh, "A self-oscillating QWITT diode mixer," *Proc. 19th European microwave conf.*, Sept. 1989, pp. 714-718.

[19] T.C.L.G. Sollner, E.R. Brown, W.D. Goodhue, and C.A. Correa, "Harmonic multiplication using resonant tunneling," *J. appl. phys.*, Vol. 64, Oct. 1988, pp. 4248-4250.

[20] Susanta Sen, Federico Capasso, Alfred Y. Cho, and Debbie Sivco, "Resonant tunneling device with multiple negative differential resistance: digital and signal processing applications with reduced circuit complexity," *IEEE transactions on electron devices*, Vol. ED-34, N0. 10, Oct. 1987, pp. 2185-2191.

[21] T.H. Kuo, H.C. Lin, R.C. Potter, and D. Shupe, *Proceedings of the 1989 IEEE cornell conference on advanced concepts in high speed semiconductor devices and circuits*, 1989, pp. 265-273.

[22] F. Capasso and R.A. Kiehl, "Resonant Tunneling transistor with quantum well base and high-energy injection: A new negative differential resistance device," *J. appl. phys.* Vol. 58, 1985, pp. 1366-1368.

[23] K. Krishnamurthi and D.R. Conn, "Conversion gain and stability of a resonant tunneling diode harmonic mixer," *Microwave and optical technology letters*, Vol. 4, No. 5, April 1991, pp. 212-216.

[24] R.J. Hwu, "Quantum well diode frequency multiplier study," *IEEE proceedings, second international symposium on space terahertz technology*, Feb. 26-28, 1991, pp. 226-237.

[25] Daniel N. Held and Anthony R. Kerr, "Conversion loss and noise of microwave an millimeter-wave mixers, Part 1 -- Theory" *IEEE trans. microwave theory tech.*, Feb. 1978, Vol. MTT-26, pp. 49-55.

[26] Daniel N. Held and Anthony R. Kerr, "Conversion loss and noise of microwave an millimeter-wave mixers, Part 2 -- Experiment" *IEEE trans. Microwave theory tech.*, Feb. 1978, Vol. MTT-26, pp. 55-61.

[27] T. Wei and S. Stapletion, "Equivalent circuit and capacitance of double barrier resonant tunneling dide," in *J. appl. phys.* Vol. 73 (2), 15 January, 1993, pp. 829-834.

[28] T. C. L. G. Sollner, E. R. Brown, C. D. Parker, and W. D. Goodhue, "High-frequency applications of resonant-tunneling diodes," in *Electronic properties of multilayers and low dimensional semiconductor structures*, J. M. Chamberlain, L. Eaves and J. C. Portal, Eds. New York: Plenum Press, vol. 231, NATO ASI series B, 1989, pp. 283-296.

[29] C. F. Edwards, "Frequency conversion by means of a nonlinear admittance," *Bell syst. tech. J.*, Vol. 35, Nov. 1956, pp. 1403-1416.

[30] E. G. Cristal, "Coupled circular cylindrical rods between parallel ground-plates," *Trans. inst. elect. electronics*, MTT-12, July 1964, pp. 428.

[31] G. Matthaei, L. Young, E. M. T. Jones, "Microwave Filters, Impedance-Matching Networks, and Coupling Structures," pp. 98-99.

[32] V. Belevitch, "Tchebyscheff Filters and Amplifier Networks," *Wireless engineer*, Vol. 29, pp. 106-110 (April 1952).

[33] H. J. Orchard, "Formula for ladder filters," *Wireless engineer*, Vol. 30, pp. 3-5.